BRNO UNIVERSITY OF TECHNOLOGY

FACULTY OF MECHANICAL ENGINEERING

INSTITUTE OF MATERIALS SCIENCE AND ENGINEERING

PROCESSING AND PROPERTIES OF 1D AND 2D BORON NITRIDE NANOMATERIALS REINFORCED GLASS COMPOSITES

SHORTER VERSION OF DOCTORAL THESIS

AUTHOR   Ing. Richa Saggar

SUPERVISOR   prof. Ing. Ivo Dlouhý, CSc.

BRNO 2016

Acknowledgements

Table of Contents

1. Introduction

Composites constitute of two or more components (matrix and reinforcements) having different set of characteristics. Various naturally occurring composites[1] acted as a motivation for engineered composites where tailoring of desirable properties of the composites could be realized. Broadly composites can be classified into three categories: ceramic matrix composites (CMC), metal matrix composites (MMC) and polymer matrix composites (PMC) depending on the type of matrix used. The properties of the different matrix composites are mentioned in Fig. 1.1. The manipulation of the microstructure during the processing stages of the composite can efficiently alter the properties of the composites to achieve desirable characteristics. The properties of the reinforcements, their concentrations and their geometries act as the key factors influencing the properties of the composites.

	Ceramic	Metal	Polymer
Hardness	⬆	⬇	⬇
Elastic modulus	⬆	⬆	⬇
High temperature strength	⬆	⬇	⬇
Thermal expansion	⬇	⬆	⬆
Ductility	⬇	⬆	⬆
Corrosion resistance	⬆	⬇	⬇
Resistance to wear	⬆	⬇	⬇
Electrical conductivity	⬍	⬆	⬇
Density	⬇	⬆	⬇
Thermal conductivity	⬍	⬆	⬇
⬆ Tendency to high values		⬇ Tendency to low values	

Fig. 1.1: Comparison of the properties of Ceramics, Metals and Polymers[2]

CMCs are considered relatively advantageous over monolithic materials as they are comparatively tougher due to several supporting phenomenas occurring due to reinforcements. Nanostructured CMCs have recently gained insight. Nanostructured CMCs are incorporated with nanosized fillers (at least one dimension is in the range of 0-100 nm). These reinforcements influence the properties of the composite to a much greater extent compared to micro sized reinforcements[3-4] including improved mechanical properties[4-5].

2. Theoretical Background

2.1. Glass and Glass Ceramic Matrix Composites

Glasses and Glass Ceramic composites offer properties like high stiffness, strength and stability at high temperatures. These properties promote them to be used in several applications like architectural, automobile and aerospace applications, telecommunication, chemical industry etc. Glasses hold several lucrative features which result in their use in the form of matrices for composites[6] :

1. Moderate range of Young's modulus for glasses allows the fillers to significantly improve the Young's modulus of the composite. This can lead to effective load transfer.
2. Glass softening at high temperatures leads to viscous flow providing ease in introducing reinforcements without any damage to the matrix to achieve high densities of composites.
3. Glasses can be easily engineered even with small changes affecting the properties drastically.
4. These matrices are cost-effective.
5. Glass matrices are free of grain, sub-grain boundaries and similar defects which makes them ideal candidate for investigation of purely the role of reinforcement.

However glass matrices suffer from the main drawback of being highly brittle with extremely low fracture toughness due to presence of defects acting as stress concentrators. Use of reinforcements like long and/or short fibres[8], particulates and platelets, whiskers reinforcement[9], laminates or layered reinforcements[10], nanomaterials[11] etc. can effectively increase the toughness of glass ceramic matrix composites[7].

2.1.1. Fibre Reinforced Glass and Glass Ceramic Composites

Reinforcement of fibres in glass matrices improve the properties like high strength, toughness, reliability and corrosion resistance, temperature resistance etc. [12] for the composites. Fibres can be classified into continuous fibres (oxide and non-oxide fibres) as well as discontinuous fibres (whiskers or short fibres), shown in Fig. 2.1. The impact of the strength of continuous fibres on the strength of a glass matrix depends on which component fails first and the relative volume fractions of matrix and fibres.

For discontinuous fibres, fibre orientation parallel to the tensile axis result in higher strength of the matrix compared to randomly oriented discontinuous fibres. The crack interaction with the weakly bonded fibres present the matrix leads to pull-out of these fibres which acts as a toughening mechanism[13]. Crack deflection is also commonly observed in fibre reinforced glass matrix composites (GMCs). Whiskers are special class

of short crystalline fibres having high aspect ratio (10-100). As reinforcements, they are very strong but they easily undergo mechanical damage (≤ 1500 MPa). SiC whiskers have been most studied in terms of application for various glass and glass ceramic matrices[14,15]. Sambell et al. showed an increase in the strength of Pyrex glass from 100 MNm^{-2} to 680 MNm^{-2} by introducing 40 vol% of carbon fibres[16].
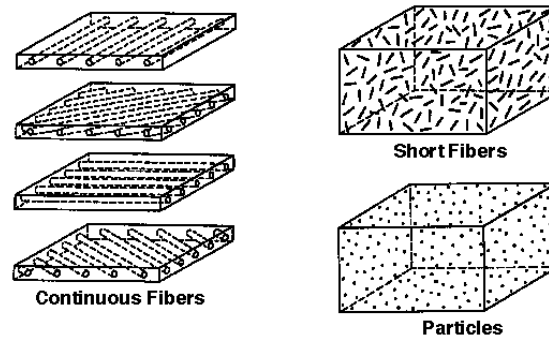

Fig. 2.1: Types of fibre reinforced composites

2.1.2. Particulate Reinforced Glass and Glass Ceramic Composites

These reinforcements do not provide considerable increase in fracture toughness or strength to glass ceramic composites but are used widely because of being cheaper and easy processing routes. Other than the mechanical properties[17], they enhance functional properties like thermal diffusivity, thermal conductivities[18], thermal shock and resistance to erosion[19] for the composites. Various forms of particles have been used as fillers, e.g. calcium carbonate, feldspar, clay, silica, graphite etc. Recently, diamond particles have been used in borosilicate glass to exploit their properties for application in high temperature devices, cutting tools etc[20].

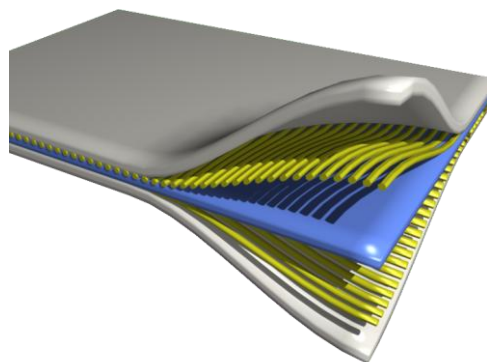### 2.1.3. Layered/Laminate Glass Ceramic Composites

Fig. 2.2: Laminated glass ceramic composite

Composites with sandwich like structure have been observed to display augmented mechanical properties compared to monolithic materials while supporting

6

different functional properties (Fig. 2.2)[10,21,22]. The use of layered ceramics or laminates can be advantageous as they provide higher wear resistance and strength due to outermost interacting homogenous layer but intrinsically they improve the toughness due to underlying heterogeneous layered structure. Glass ceramic multilayered composites have found their applications in microelectronics industry[23] as they offer highly preferable characteristics including thermal, electrical as well as mechanical properties[24] and armour materials[25].

2.1.4. Nanocomposites

Due to the high aspect ratio of nanomaterials, nanocomposites offer improved functional and mechanical properties in comparison to conventionally reinforced composites due to better interfacial interaction between reinforcements and matrix with a very concentrations of reinforcements[26]. The nanosized reinforcements can be classified into zero dimensional (0D; nanoparticles), one dimensional (1D; nanotubes) and two dimensional (2D; nanosheets) as shown in Fig. 2.3.
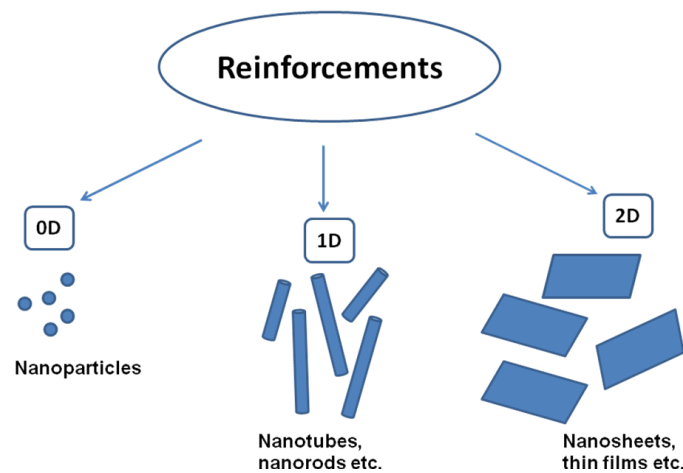
Fig. 2.3: Types of reinforcements used in nanocomposites

2.1.4.1. 0D nanocomposites

0D nanocomposites consist of reinforcements confined in all the dimensions to nano-range ($\leq$ 100 nm). They mainly constitute of nanoparticles mainly produced by sol-gel technique[27,28]. Niihara et al. reinforced SiC nanoparticles in Al_2O_3, MgO and Si_3N_4[3] to improve the mechanical properties. However, these reinforcements suffer from agglomeration problem at high concentrations and they offer lesser surface area for interaction with the matrix in comparison to 1D and 2D nanomaterials[29]. As mechanical reinforcements, they do not provide complete justice to crack defence mechanisms due to the geometric limitations.

2.1.4.2. 1D nanocomposites

Reinforcements in 1D nanocomposites are confined in one dimension in nano-range. Carbon Nanotubes (CNT) as 1D reinforcements, offer several functional properties to the glass composites including high aspect ratio, high Young's modulus (1300 GPa), high tensile strength (20-63 GPa), higher electrical conductivity (10^7 S/m) and high thermal conductivity (1800-6000 W/mK) but they suffer from drawbacks like agglomeration and entanglement[30] and low thermal stability[31]. CNT have shown some potential in the toughening of glass and ceramic matrices[4,53,32,33,34]. 1D nanofillers like nanotubes possess, in general, geometrical advantage over nanoparticles as they are able to hinder the crack propagation in a direction perpendicular to the length of the nanotubes. The reinforcement of barium aluminosilicate glass by 10 vol% CNT produced 143% increase in fracture toughness in the composite[33].
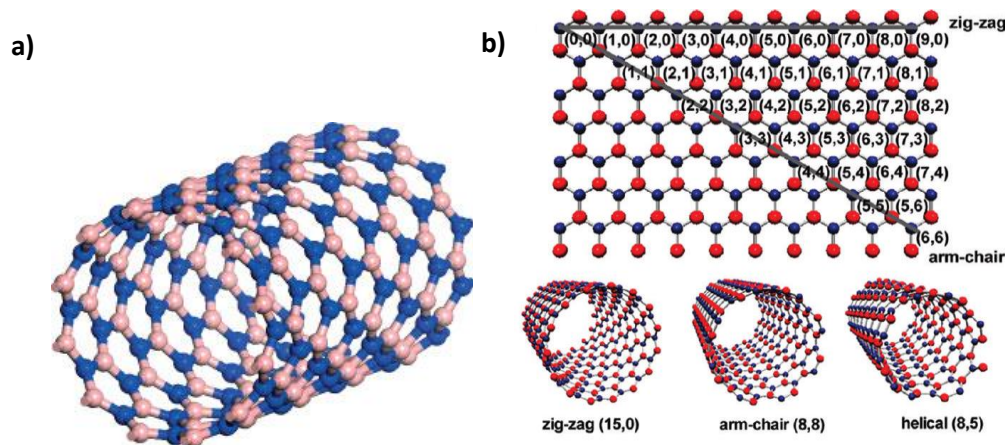
2.1.4.2.1. Boron Nitride Nanotubes

Fig. 2.4: a) Model of BNNT structure with adjacent boron and nitrogen atoms[38] ; b) Chiralities of single walled BNNTs indicating their (n,m) indices for rolling direction[39]

BNNTs structure is analogous to hexagonal comb structure present in CNTs having adjacent B and N atoms[35,36,37] (Fig. 2.4(a))[38]. BNNTs can be single walled or multi walled posessing partially ionic B-N bonds. Various researchers have reported that the distance between the layers in hexagonal multi walled BNNTs ≥ 0.333 nm. BNNTs support three chiralities according to the direction of rolling of boron nitride atomic layers: zig zag, arm chair and helical (Fig. 2.4(b)), zig zag being most common. They are crystalline[39], electrically insulating (band gap-5.5 eV [40]) and they exhibit comparable stiffness[38], elastic modulus[41,42], yield strength[43] and thermal conductivity[44,45], high tensile strength to CNTs[46]. Additionally, individual BNNTs can withstand comparatively higher external tensile load[47] and are better shock absorbers[48] than CNTs. They are thermally stable up to 950 °C and hence are considered chemically inert[38]. Due to these properties, they have been investigated in different matrices like metals[49], polymers[50,51],

biomaterials[52], glasses[8,53,54] and ceramics[55,56,57] to enhance the mechanical and thermal properties of the matrices.

2.1.4.3. 2D nanocomposites

Reinforcements used in 2D nanocomposites are confined in two dimensions in nano-range. They offer toughening along two dimensions at reinforcement-matrix interface. A deeper insight in 2D reinforcements developed with the discovery of graphene by Novoselov et al.[58] Graphene exhibited similar electrical, thermal and mechanical properties[59,60] as its 1D analogue (CNTs)[61,62]. However, 2D structure of graphene sheets possessed higher surface area[63] and less probability of entanglement (or agglomeration)[64] over CNTs and hence have comparatively better properties than CNTs. Porwal et al.[11] reported ~35% increase in the fracture toughness for graphene reinforced SiO_2 glass by using 2.5 vol% of concentration for graphene[11].

2.1.4.3.1. Boron Nitride Nanosheets
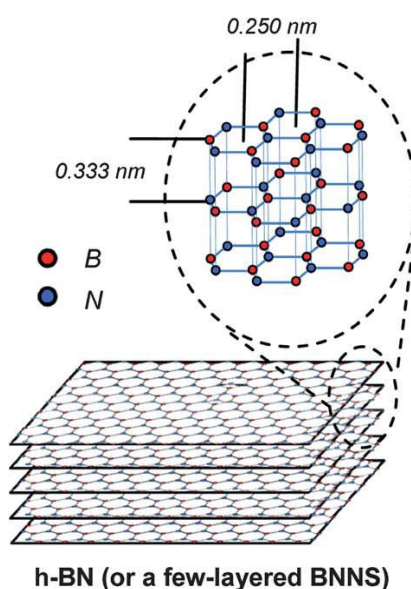
Fig. 2.5: Structure of 2D BNNS [65]

Boron nitride nanosheets (BNNSs) possess similar functional properties to BNNTs, while differing in geometrical properties, similar as graphene and CNTs[11]. They are structural analogues of graphene. Boron nitride nanosheets are formed by honeycomb network of borazine ($B_3N_3H_6$) with covalent B-N bonds (slight ionic in nature) with a bond length of 1.45 nm and the distance between centre of adjacent rings being 2.50 nm (Fig. 2.5.)[65]. They possess zig zag, arm chair and helical chirality. The layers of BNNSs have weak Van der Waals forces in between them with interlayer distance of 0.333 nm. Owing to the two-dimensional geometry, BNNSs provide advantages like higher specific surface area[66,67] lesser entanglement and toughening in

two dimensions in composites. The methods to synthesise BNNSs are far more convenient, cost effective and give a better yield compared to BNNTs[39]. Lee et al.[68] reported the enhancement of 24.7% toughness, 9.4% strength and 26.7% tribological properties for Si_3N_4 by reinforcing 2 vol% concentration of boron nitride nanoplatelets. To the best of our knowledge, BNNSs have not been used in glass matrices and would be reported as a mechanical reinforcement for glasses in this work.

2.2. Processing of Glass Ceramic Composites

Good dispersion of the reinforcements remains a primary challenge during processing of ceramic matrix composites. Particularly for the processing of nanocomposites, uniform dispersion of nanofillers affects the final properties of the nanocomposites as the nanofillers have the tendency to agglomerate due to high surface energy which deteriorates the properties of the bulk composite material.

2.2.1. Powder Processing

This is the most conventional method used for processing the glass ceramics. It has been used for number of reinforcements like CNTs[69], BNNTs[5], graphene[70], boron nitride nanoplatelets or BNNS[68] for different matrices like barium calcium aluminosilicate glass[5], alumina[71], zirconia[55], Si_3N_4[68], silica[11] etc. producing mixed results depending on the reinforcement of these nanofillers and the matrix. The basic methodology for the powder processing involves selection of components with desirable properties for the composites and their processing through milling, washing n filtering for consolidating through sintering[72,73]. The methodology may also include pre-processing of the precursors with the help of ultrasonication or mechanical mixing for achieving better dispersion of the fillers post sintering in the matrix. It is an energy effective processing method. The milling conditions play a crucial role in uniform dispersion of reinforcement into the matrix. Preparation of BNNTs based nanocomposites have been reported in 3Y-TZP zirconia[55] by ball milling method. Porwal et al.[11] reported uniform dispersion of graphene and graphene oxide nanoplatelets by their dispersion in Dimethylformamide (DMF) by sonication and then mixing them with silica glass relative density of >99%.

2.2.2. Colloidal Processing

Colloidal processing based composites involve multiphase system in the form of continuous dispersions having variety of particle size ranging from nano- to micro-size. Broadly, the colloidal dispersions were classified into: solid, liquid and gaseous, depending on dispersed phase and dispersion medium. Generally, for glass and ceramics, powders are suspended in liquid medium for colloidal processing. During colloidal processing the particles have a tendency to aggregate. Stabilization of the suspension is achieved by creating repulsion between the particles by electrostatic

mechanism by providing interaction between like charged particles by dispersing in polar medium or by coating the particles with the polymer to avoid aggregation. However, the use of polymers in the composite formation may affect the properties of the consolidated sample on a macro scale and moreover it is not easy to completely remove this polymer on the later stages. Wang et al. successfully produced graphene based ceramic nanocomposites by adding graphene oxide suspension to alumina suspension while mixing with resulting composite achieving 53% increased fracture toughness and 13 order higher electrical conductivity compared to pure alumina[74].

2.2.3. Sol-Gel Processing

The sol-gel processing is highly homogenous and maintains high purity of the composite. It is flexible process in terms of shaping the final composites as the precursors are liquids. In general, it comprises of four stages: sol formation, gelation, drying and densification[75]. The metal alkoxide precursors hydrolyze and condense forming a colloidal sol and are used as a precursor. As the liquid sol is condensed, the solid phase starts to develop a network, converting it to gel form. Sol-gel transformation is an irreversible process. With the continual evaporation of liquid, the gel transforms to xerogel which can be densified using various sintering techniques. Sol-gel process can be combined with other processing methods like powder processing. This process is most common for preparation of silica based composites for various application[76,77]. Watcharotone et al.[78] reported preparation of graphene-silica films to be used as transparent conductors.

2.2.4. Polymer Derived Ceramics

Polymer derived ceramics (PDC) processing technique enables the development of ceramic fibres, coating or layers which are stable at high temperatures with respect to decomposition, crystallization and phase separation. These ceramics are high purity and support homogeneity. The processing includes two major steps: 1) Evaporation: preparation of pre-ceramic polymers from suitable monomers and cross linking of pre-ceramic polymer to form organic/inorganic network; 2) Pyrolysis process (conversion to ceramics) by use of moderate temperature (1000-1300 °C). This process results in amorphous covalent ceramics which could be crystallized at higher temperatures. PDC could be used for preparation of glass ceramic nanocomposites as preparation of nanofillers like CNTs, graphene, boron nitride nanotubes[79] is easy by pyrolysis of suitable liquid precursors. Ji et al.[80] reported preparation graphene and silicon oxycarbide composites by using PDC technique with up to 30 wt% loading of graphene oxide powder in polysiloxane for application as anode in Li ion batteries.

2.3. Sintering of Glass Ceramic Composites

Sintering can be defined as increasing the contact area between particulates by using relevant conditions like temperature, pressure and surrounding environment for transporting of the material to the pores and its surrounding[81]. Successful sintering procedures can lead to highly dense samples which is aimed for uniformity in properties of the sample. Basic methodology of sintering for consolidating the glass ceramics is presented in Fig. 2.6.
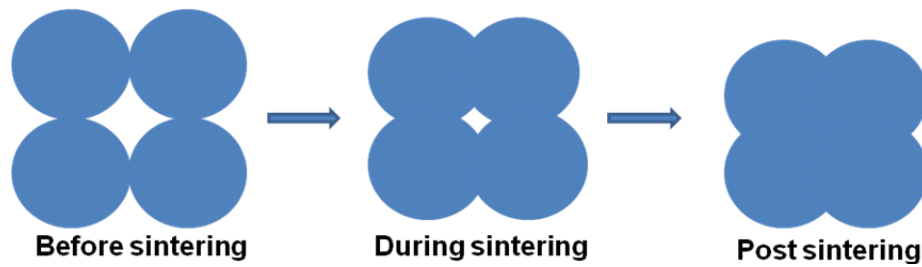

Fig. 2.6: Basic sintering methodology for densifying glass ceramics

2.3.1. Conventional Sintering Techniques

Conventional sintering techniques include methods like pressureless sintering where high temperatures and prolonged sintering time are applied to achieve high density composites. However, use of conventional sintering techniques lead to grain growth in ceramics and also adversely affect the nanofillers used as reinforcements[82,83]. Michalek et al. reported aqueous slip casting of alumina and 0.1 wt% MWCNTs[32] composites by pressureless sintering methods achieving 99.9% density at 1500 °C but no improvement in the mechanical properties was observed compared to monolithic alumina matrix.

2.3.2. Two Step Sintering

Two-step sintering is a relatively simpler sintering technique with application of lower temperature to achieve higher density with slower grain growth in comparison to conventional sintering technique. In the first step, the powder sample was heated to a higher temperature to make the sample dense enough (>75%) to ensure good nucleation and initiation of crystal growth and then the temperature was subsequently decreased to achieve a fully dense sample without changing the grain size of the ceramic sample with constant heating rate cycle. Chen et al.[84] reported the sintering of yttria stabilized zirconia by studying the shrinkage data by maintaining constant heating rate and obtained high density (~95%) for tetragonal $(ZrO_2)_{0.97}(Y_2O_3)_{0.03}$ and cubic $(ZrO_2)_{0.92}(Y_2O_3)_{0.08}$ ceramics with nanocrystalline and sub-microcrystalline structures. Though, this technique is simpler yet uniformity in the densities of different phases of the matrix during transformation (if not controlled) can serve as a drawback. Also, the

grain growth in the final stage of sintering is questionable for achieving highly dense samples[85].

2.3.3. Stress Assisted Sintering Techniques

These sintering methods take advantage of external compressive stresses in order to lower the sintering temperatures. Though widely used, the use of high temperature can lead to degradation of nano reinforcements and grain growth.

2.3.3.1. Hot Pressing

Hot pressing involves use of high pressure piston on the powder confined in a die while simultaneously applying high temperature to achieve pore-free highly dense samples. Boccaccini et al.[86] reported borosilicate glass composite reinforced with 10 wt% of MWCNTs by sol-gel process densified by using pressureless sintering and hot pressing. It was reported that cold pressing could not densify the sample to a great extent but with hot pressing of the composite, higher densities were achieved.

2.3.3.2. Hot Isostatic Pressing (HIP)

During hot isostatic pressing, the powder is constrained in a isolated membrane like structure and a high pressure gas, generally argon due to its inert nature, is applied to generate hydrostatic compressive stresses uniformly in all the directions[87]. HIP can be used to sinter complex shapes. Li et al. prepared bio-ceramics of partially stabilized zirconia (PSZ) with hydroxyapatite (HA) by HIP by applying 160 MPa pressure at 1225 °C. HA did not suffer from much degradation and 97% theoretical density was observed for HIP sintered samples[88].

2.3.4. Field Assisted Sintering Techniques (FAST)

FAST is advantageous due to fast heating rate, low dwelling period, no sintering aid requirement, lower temperatures required and no pre-loading required.

2.3.4.1. Spark Plasma Sintering

Spark plasma sintering (SPS) uses the rapidly changing electric field for the sintering process. Rapid sintering by SPS aids in the sintering of composites without affecting the properties of the reinforcements or matrix. In this process, electric current affects the temperature which advances to Joule heating spread all over the specimen while simultaneously applying high pressure up to 1 GPa[89]. Smaller holding time (3-10 min), lesser sintering temperature and high heating rate (~100 °C/minute) during SPS lead to greater hold on the microstructure of the glasses and ceramics. The entire process is carried out in vacuum condition. Alignment of reinforcements perpendicular to the direction of applied pressure have been been observed for SPS

sintered samples[90]. Centeno et al. confirmed such behaviour for graphene reinforced alumina composites[90] by Raman spectroscopy. The apparatus for carrying out SPS for composite samples is presented in Fig. 2.7.

Fig. 2.7: Spark plasma Sintering apparatus

2.3.4.2. Microwave Sintering Technique

Microwave sintering is another fast sintering process which uses low temperature and high speed sintering. In general, the kinetics of the microwave sintering technique is two-three folds higher when the conventional heating is replaced with microwaves[91]. During this process, the ceramic powders to be sintered are surrounded by the susceptors of microwaves, e.g. ferric oxide which transform the microwaves into heat. Since the specimen generates heat in itself, the heating is rapid and selective thereby achieving high heating rates in shorter durations. The faster sintering process does not allow grain growth in high amount as well as avoids formation of intermediate changes thus reducing the chances of their adverse effects in the final ceramic product. Alumina reinforced with 5 vol% of zirconia achieved a density of 99% within 35 minutes[92]. At room temperature, the conventional low frequency (2.4 GHz) microwave applicators applicators do not efficiently couple microwaves to ceramics and therefore causing difficulty in initial heating of the samples and thermal instability can affect the properties of the composites. Therefore, collaborated with infrared source, it provides the pre-heating of the ceramics to their critical temperature after which microwave heating takes over and is sufficient[93].

3. Aim of the work

The main task of the thesis work deals with the study of reinforcement of glass ceramic composites to enhance their mechanical properties in comparison to monolithic glass ceramics. For this purpose, the work is mainly focused on boron nitride 1D and 2D reinforcements namely boron nitride nanotubes (BNNT) and boron nitride nanosheets (BNNS). The tasks of the thesis work were broadly categorized into:

1) Characterization of the commercially obtained BNNT to study the morphology and structure of the BNNT. Detailed studies to understand the elemental analysis, purity, temperature dependence, density etc. for the commercially obtained BNNT. Necessary steps taken to make them more readily usable and yield maximum benefits in the composite matrix contributing to enhancement in the mechanical properties of nanocomposite matrix.

2) Synthesis and optimization of conditions to produce high quality BNNS by liquid phase exfoliation technique with high aspect ratio. Characterization of the morphology and properties of as-prepared BNNSs using Scanning Electron Microscope, Transmission Electron Microscope, X-Ray Diffraction, Thermo-gravimetric Analysis, Fourier Transform Infrared Spectroscopy, density analysis etc.

3) Preparation and processing of borosilicate glass (BS) - BNNT (BS-BNNT) as well BS and BNNS (BS-BNNS) composite powders by powder processing method and optimizing the conditions of Spark Plasma Sintering process for densification of the composite powders by reinforcing different concentrations of BNNTs and BNNSs.

4) Ceramographic preparation for the bulk composite samples and study of the mechanical properties of the bulk composite matrix. The mechanical properties include the density, Young's modulus, micro-hardness, fracture mechanics, flexural strength, tribological properties etc.

5) Thorough investigation of the microstructure as well as the fracture micro-mechanics and micro-mechanisms developed in the matrices after the mechanical testing including observation of fractured surfaces after the testing using optical microscope, scanning electron microscope and other techniques.

4. Materials and Methods

4.1. Borosilicate Glass

Commercially available borosilicate glass powder (BS; glass type GM27884: 55 wt% SiO_2–25 wt% BaO–10 wt% B_2O_3–10 wt% Al_2O_3; Schott NanoFine NF180, Germany) was used as the matrix for the glass composites. The glass transition temperature of the BS powder used was 665 °C, and the particle size (d_{50}) was 183 nm.

4.2. Boron Nitride Nanotubes (BNNTs)

Boron Nitride Nanotubes (BNNTs) were purchased from School of Materials Science and Engineering, Wuhan Institute of Technology in China. These BNNTs were prepared by self-propagation high-temperature synthesis (SHS) and further annealed using CVD process[94]. Two types of BNNTs were obtained differing in morphology, thereby used as reinforcements, namely, hollow cylindrical type (BNNT-C) and bamboo type (BNNT-B) with bamboo like knots in between. The BNNTs obtained were of similar diameter, i.e. 10 nm ≤ d ≤ 100 nm but varied in lengths as BNNT-C (≥ 10 μm) were approximately double the length of BNNT-B (≥ 5 μm).

4.2.1. Purification of BNNTs

The as-received BNNTs were purified by leaching process by treating them with 5M HCl solution at 90°C for 5 hours with magnetic stirring. This process helped in the removal of iron impurities present in the BNNTs, used as a catalyst during BNNT growth process. Thorough stirring of the solution lead to appearance of green colour in the solution signifying the removal of iron in the form of iron chloride (as shown in equation 4.1).

$$Fe + 2HCl \rightarrow FeCl_2 (Green) + H_2 \qquad (4.1)$$
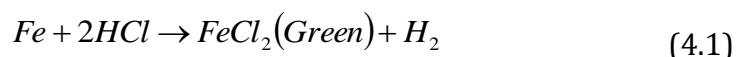
The resultant solution was filtered using 0.22 μm Millex PTFE filter (Millipore Corp., Ireland) separating the purified BNNTs from the solution. This process was again repeated with 1M HNO_3 acid in order to remove the magnesium impurities from BNNTs in the form of magnesium nitrate salt. The resulting purified BNNTs were re-filtered and were washed thoroughly with deionized water for washing out traces of acid present on the walls of BNNTs.

4.3. Boron Nitride Nanosheets (BNNSs)

Boron nitride nanosheets (BNNSs) were used as another form of reinforcements in the BS glass matrix prepared by liquid exfoliation process. Hexagonal boron nitride powder (h-BN; PT110, Momentive Ceramics Strongsville, Mean particle size d_{50} ~47 μm) was used for the preparation of BNNSs. Exfoliation of h-BN precursor powder

was carried out by dispersion of h-BN in N-methyl-2-pyrrolidone (NMP) with 100 mg/ml concentration using a high power tip sonicator (CV33 flat probe sonic tip, 50 W, 25 kHz) for 24 hours. The suspension was surrounded by an ice bath to prevent the oxidative degradation of NMP. After 24 hours, the sonicated suspension was centrifuged (Centurion Scientific) at 500 rotations for 45 minutes to separate the supernatant containing lighter BNNSs from heavier bulk h-BN powder that settled down. The supernatant was vacuum filtered and the collected BNNSs were washed with ethanol and water repeatedly to remove the traces of residual NMP stuck on the BNNSs surface. NMP was considered favourable as a solvent for the liquid phase exfoliation purpose due to higher boiling point (~200 °C) which facilitates in using high power sonication tip without any harm to the dispersing solvent. Moreover, NMP being highly polar solvent aided in de-aggregation of BNNSs.

5. Powder Processing for Composite Mixtures

5.1. BS-BNNT Composite

BS-BNNT composites were prepared with the as-received BNNTs and purified BNNTs with the concentrations of 0 wt%, 2.5 wt% and 5 wt% of BNNTs respectively. In order to prepare BS-BNNT composites, BNNTs were suspended in ethanol with concentration of 1 mg/ml by ultrasonicated for 2-3 hours. The well-dispersed BNNT suspension was added to BS powder to prepare composite slurries by planetary ball mill (Pulverisette, Fritsch) for 12 hours using BS glass balls (3 mm and 10 mm; Duran®, Ginzel s.r.o., Czech Republic) at 350 rpm. The powder to ball weight ratio used was 1:20. Post milling, the slurries were dried in oven in ambient atmosphere at 100 °C to remove residual ethanol. The dried powders from slurries were collected, crushed and screened through 100-mesh sieve to obtain fine composite powders followed by heating the powders again at 300 °C for 3 hours to remove the traces of any trapped ethanol in the dried and crushed composite powders.

5.2. BS-BNNS Composite

For preparation of BS-BNNS composites, the BNNSs were suspended in ethanol using ultrasonic probe for 2 hours to form a uniform suspension. This suspension was added to BS powder for the preparation of 0 wt%, 2.5 wt% (BS-BNNS (2.5 wt%)) and 5 wt% BNNSs (BS-BNNS (5 wt%)) reinforced BS glass. These mixtures were ball milled with ethanol as a solvent for 6 hours at 350 rpm using 3 mm and 10 mm zirconia balls (YTZ® grinding media, Tosoh Corporation, Japan) by planetary mill. The powder to ball weight ratio used was 1:25. Different sizes of milling balls were employed to ensure uniform and fine mixing of the mixtures[95]. The slurries hence produced were dried in oven in ambient atmosphere at 100 °C to obtain composite powders which were crushed and sieved through 250 mesh sieve. Thereafter, the fine powders were dried at 300 °C for removal of excess ethanol trapped in the composite powder for 24 hours.

5.3. Sintering of Nanocomposites

The composite powders for BS-BNNT composite and BS-BNNS composite, post drying process, were consolidated into a disc shaped samples using SPS (HPD 25/1, FCT systems, Germany) by placing the preloaded powders by pressing machine in graphite die. This graphite die with pressed powders was loaded in SPS furnace. During SPS high electric DC currents were applied to achieve high temperatures with simultaneous application of high pressure. The composite powders for BS and concentrations of BS-BNNT and BS-BNNS were sintered at 775 °C for a dwell time of 7 minute while applying 40 MPa pressure in vacuum. The heating and cooling rates used for the SPS process were 50 °C/minute. High heating rates and vacuum environment during SPS process avoided any damage to nano reinforcements during high temperature processing. The conditions of the sintering were slightly altered for each concentration in order to achieve highest relative density possible. Fig. 5.1. shows the sintering profile of parameters for BS + 2.5 wt% BNNT-B which shows the rate of change of sintering temperature (in black), the average speed of the piston (in blue), the force applied by the piston on the composite powder present in the die (in green) and the displacement of piston with time (in red). The disc samples were obtained with a diameter of 20 mm and with a thickness of ~3 mm. These disc samples were further machined into 2 mm × 3 mm × 20 mm dimensional bars and their surfaces were prepared by grinding and polishing for the mechanical tests.
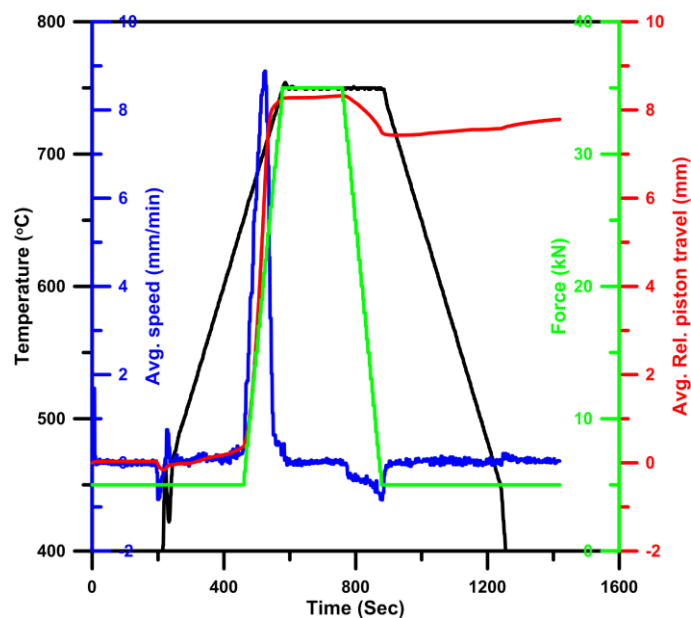

Fig. 5.1: Spark plasma sintering parameters profile for BS + 2.5 wt% BNNT-B

5.4. Characterizations

Field emission gun SEM (Tescan Lyra 3 XMU, Czech Republic) integrated with EDS unit was used to study the structure and morphology of the purified BNNTs,

produced BNNS as well as pure BS, BS-BNNT and BS-BNNS composite powders produced. This technique was also used to analyze the fracture surfaces after the flexural strength and for measurement of fracture toughness by chevron notch measurements.

Transmission Electron Microscopy (TEM) was carried out on JEOL JSM-2010 using the carbon grids for studying the morphology and of the BNNS produced.

Density of the purified BNNTs as well as produced BNNS was measured by helium pycnometer (AccuPyc II 1340 Pycnometer). The densities of the bulk sintered composite samples were measured using Archimedes principle. The density of the BS powder used for the calculation of theoretical density was 2.8 g/cm³ (provided by the powder supplier).

The XRD analysis of both the bulk sintered samples and the as produced BNNSs powder were performed using X'Pert diffractometer (Panalytical) using Co Kα radiation with a β filter in the secondary beam.

The elastic modulus of the samples was measured using the impulse excitation resonance method using GrindoSonic Mk5i (J.W. Lemmens N.V., Belgium) by acoustic detector. A mean value of 15 recorded measurement frequencies for each sample was considered.

A computer-controlled microhardness tester (Zwick/Roell Indentec ZHV, at 1 kg for 10 s) was used for determination of microhardness and indentation fracture toughness (equation 6.1.) of BNNT/borosilicate Glass composites. Minimally, 10 measurements were carried out on each sample. Fig. 5.2. shows the scheme of the indent formed by the Vickers indenter.
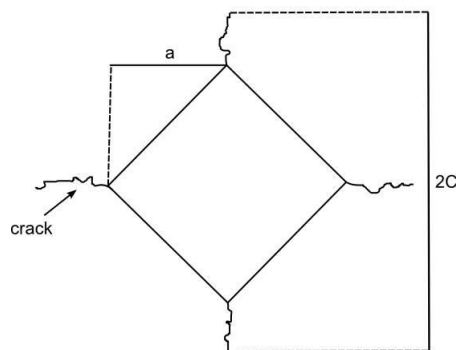
$$K_{1C} = 0.0154 \times \left(\frac{E}{H} \right)^{1/2} \times \left(\frac{P}{C^{3/2}} \right).$$

(6.1)

Fig 5.2: Scheme of the indent formed by Vickers indentation

Where E is Young's modulus, H is hardness, P is load, and C is average radial crack length. To apply the equation, experimental Vickers hardness and elastic modulus values were determined for each BNNT reinforced borosilicate composite samples.

The fracture toughness for the BS and the composite samples was measured on polished bars with rectangular nominal dimensions of 2x3 mm by chevron notch technique. The samples were tested on a universal testing system, Instron 8862 (Instron, USA), by three-point bending with 16 mm span and at a crosshead speed of 1 μm/min and was calculated by equation 6.2:

$$K_{Ic} = \frac{F_{max} \cdot Y_{min}^{*}}{BW^{1/2}}.$$ (6.2)

Where F_{max} is the maximum force determined from the load–deflection trace, Y^*min is the minimum of geometrical compliance function Y^*_{min},[96] and B and W are the thickness and height of the sample respectively. At least three beams were tested for each composition.

The flexural strength of the BS and composite samples bars was measured on highly polished bars by universal testing system, Instron 8862 (Instron, USA), on a 16 mm span with a crosshead speed of 100 mm/min. At least three specimens were measured for each composite concentration. The flexural strength of the sample bars was calculated by equation 6.3 using the following standard (EN 843-1:1995):

$$\sigma_f = \frac{3F_m \cdot l}{2bh^2}.$$ (6.3)

Where F_m denotes the maximum force, l is the distance between the centres of outer support rollers in a three point bending set-up (expressed in mm), b is the width, and h is the thickness (dimension in crack propagation direction; expressed in mm) of the specimen.

Scratch testing for the BS-BNNT composites was analyzed by UMT Multi-Specimen Test System (Bruker, USA) scratch tester. Vickers indenter was used for the measurement with a increasing force from 0.5 N to 2 N employing a constant speed of 0.1 mm/sec for the indenter displacement length of 2 mm on the composite sample. 3 measurements were recorded for each set of sample.

The wear behaviour of the BNNSs reinforced BS glass was analyzed by the help of DTHT 70010 tribometer (CSM Instrument, Switzerland) using non-lubricated ball-on-disc method (ASTMG99-03) by BS ball and alumina ball. The tests were conducted with a normal force of 1 N by ball on the polished surface of the composite for both types of balls at room temperature employing a speed of 0.1 m/s for a track

displacement of 500 m. Specific wear rate (equation 6.4) is defined as worn volume (V) per unit loading force (F_p) per unit sliding distance (L), i.e.

$$r = \frac{V}{F_p \cdot L} \left[\frac{mm^3}{Nm} \right]. \qquad (6.4)$$

7. Main Results

7.1. BS-BNNT composites

7.1.1. Material Analysis

The BNNTs procured from Wuhan Institute of technology were observed using SEM. The detailed SEM images of the BNNTs produced are presented in Fig. 7.1.
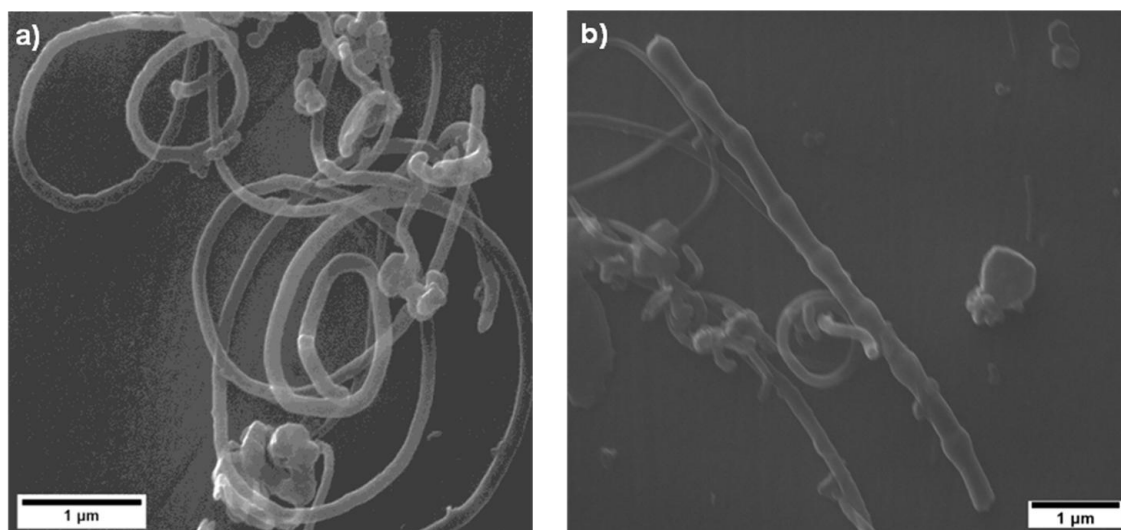

Fig. 7.1a) Cylinderical Boron nitride Nanotubes; b) Bamboo like boron nitride nanotubes

The density of the boron nitride nanotubes were measured using helium pycnometer. The value of densities of BNNT-B and BNNT-C were 2.1093 g/cm^3 and 2.1417 g/cm^3. The zeta-potential observed for neutral (pH ~7) BNNTs in ethanol was -17.9 while the BS zeta-potential was -21.3. This ensured the dispersion of BNNTs uniformly in BS with limited agglomeration. Thermo-gravimetric measurements show that the BNNTs were stable until 600 °C with a 3% weight loss.

7.1.2. Microstructure analysis

The relative densities of the Pure BS, BS-BNNT (2.5 wt%) and BS-BNNT (5 wt%) are given in Table 7.1.

Table 7.1: Values of densities for 0 wt%, 2.5wt% and 5wt% of BS-BNNT using bamboo like and cylindrical nanotubes

Relative Density	0 wt%	2.5 wt%	5wt%
BNNT-C	99.4 %	97.6%	97.2%
BNNT-B	(Pure borosilicate)	98.1%	97.1%

The powders of the composites were analyzed using SEM to observe the dispersion of BNNTs in the BS borosilicate matrix. The BNNT were found to be evenly

distributed in the matrix and even with 12 hours of ball milling, there was no significant damage to the BNNTs.

7.1.3. Mechanical Properties

The value of indentation fracture toughness for the pure borosilicate glass sample, as-received BNNT-C reinforced borosilicate glass (0 wt%, 2.5 wt%, 5 wt%) and as-received BNNT-B reinforced borosilicate glass (0 wt%, 2.5 wt%, 5 wt%) are presented in Table 7.2 below. An increase of 29% of indentation fracture toughness with 5 wt% reinforcement concentration of as-received BNNT was observed for the composite samples.

Table 7.2: Indentation fracture toughness of as received BNNT reinforced BS glass composite

($MPam^{1/2}$)	0 wt%	2.5 wt%	5 wt%
BNNT-C	0.851 ± 0.027	0.997 ± 0.065	1.099 ± 0.062
BNNT-B	(Pure borosilicate)	0.933 ± 0.044	1.101 ± 0.069

We observed that the values of fracture toughness for as-received BNNT reinforced borosilicate composite samples measured by chevron notch beam fracture toughness (CNF) are lower or equal to the values of pure borosilicate glass samples (Table 7.3).

Table 7.3: Fracture toughness by chevron notch measured for as received BNNT reinforced BS Glass Composite

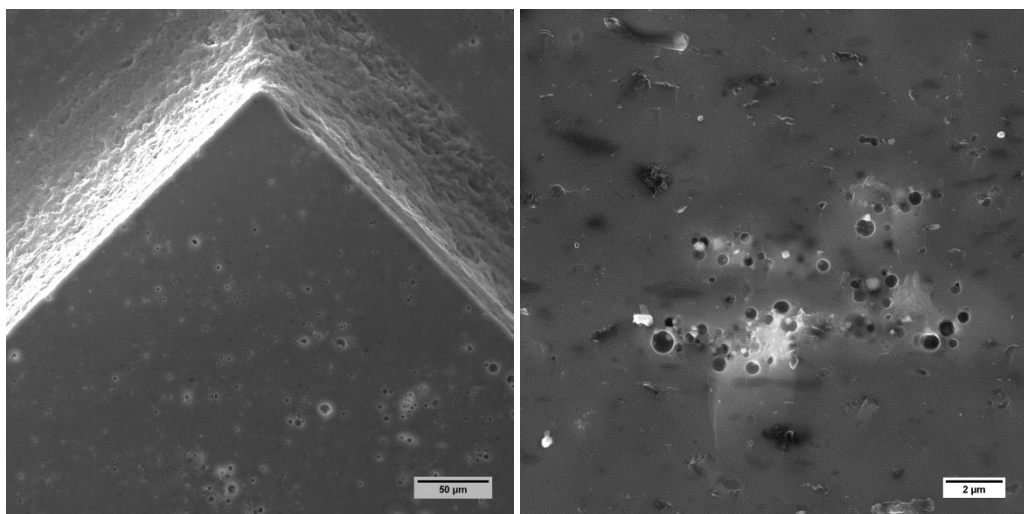| $MPam^{1/2}$	0 wt%	2.5 wt%	5 wt%
BNNT-C	0.821 ± 0.0544	0.867 ± 0.05	0661 ± 0.07
BNNT-B	(Pure borosilicate)	0.911 ± 0.04	0.723 ± 0.08

Fig. 7.2: Presence of holes in the fractured surfaces of BS-BNNT composites.

Fracture surfaces were analyzed using SEM and it was found that there were presence of many small pores on fracture surfaces (Fig. 7.2.). These pores aided the

crack propagation and hence the values of bulk fracture toughness were lower. In case of indentation fracture toughness, specific areas where no or less holes were observed were selected and the indents were made with lower weights to check the toughness of the sample which supports the idea of increase in fracture toughness. By EDS of the samples, presence of ~55% of Fe was found in the samples (Fig. 7.3.) which might be the reason of pore creation during sintering as many Fe salts based foaming agents are known to exist. This lead to the step of purification of BNNT by leaching process, reducing the amount of Fe to 1% in the BNNTs.
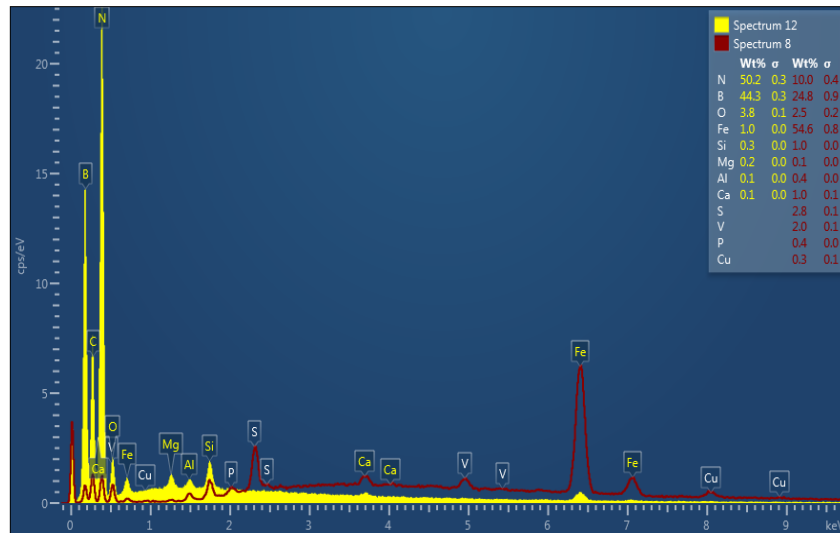

Fig. 7.3: Comparative EDS of as-received BNNT-C (yellow) and purified BNNT-C (red)

After the purification process of BNNT and composites preparation with purified BNNTs, Young's modulus, hardness values and fracture toughness measured by chevron notched beams were measured and the values are given in Table 7.4 and graphically represented in Fig. 7.4. Fracture toughness increased by nearly 25% by reinforcing 5 wt% BNNTs which confirmed the negative effect of presence of Fe in composites prepared by as received BNNTs. The toughening mechanisms developed were studied using SEM.

Table 7.4: Young's modulus and Vickers hardness for 0 wt%, 2.5 wt% and 5 wt% of BS-BNNT using purified bamboo like and cylindrical nanotubes

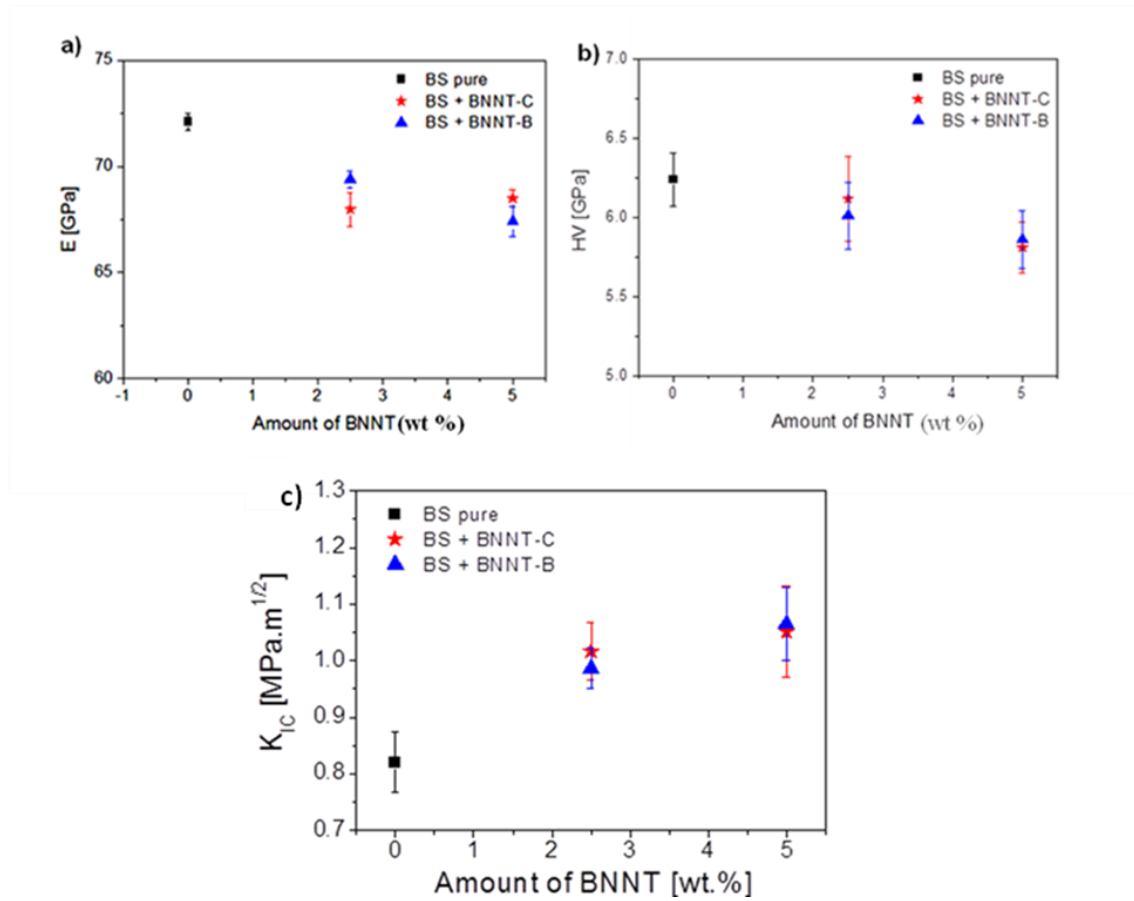| Material	Young's modulus (GPa)	Vickers Hardness HV 1 (GPa)	Fracture toughness (MPam$^{1/2}$)
BS Pure	72.1 ± 0.4	6.24 ± 0.17	0. 85 ± 0.03
BS-2.5 wt% BNNT-C	69.4 ± 0.4	6.12 ± 0.27	1.02 ± 0.05
BS-2.5 wt% BNNT-B	68.5 ± 0.8	6.01 ± 0.21	0.99 ± 0.03
BS-5 wt% BNNT-C	68.0 ± 0.4	5.81 ± 0.16	1.05 ± 0.08
BS-5 wt% BNNT-B	67.4 ± 0.7	5.86 ± 0.18	1.06 ± 0.06

Fig. 7.4: a) Young's modulus b) Vickers hardness and c) Fracture toughness by chevron notch measured for purified BNNT-C and BNNT-B reinforced BS glass composite for 0 wt%, 2.5wt% and 5 wt% concentration

BNNTs were found to be uniformly dispersed and random aligned therefore, it was believed that isotropic properties developed in the matrix. Fig. 7.5. depicts the significant toughening mechanisms like pull-out and crack bridging and observed in BNNTs reinforced BS composites. Pull-out was regularly observed in the matrix signifying uniform dispersion of BNNTs. It was also observed that with pull-out some of the matrix material also got pulled out in the process showing strong interface between the matrix and BNNT which is in agreement with the behaviour of BNNT in amorphous glass matrices[47] which helped in matrix relaxation. Due to multiwalled structure, the nanotubes also experienced "sword-in-sheath" mechanism, pulling out the weak inner nanotubes held by Van der Waals forces which helped in energy dissipation[55].

Additional toughening mechanisms observed were crack deflection and crack bridging. Crack thickness for pure BS in the vicinity of the indent was ~ 450-490 nm whereas for the composite the crack thickness in the vicinity of the indent was ~220-290 nm which shows that the BNNT bridged the crack even on the maximum while stretching but not fracturing. This stretching has not been observed for any other nanotubes (including CNTs) therefore this can be reported as a novel report of such toughening mechanism. All these toughening mechanisms lead to significant fracture toughness enhancement.
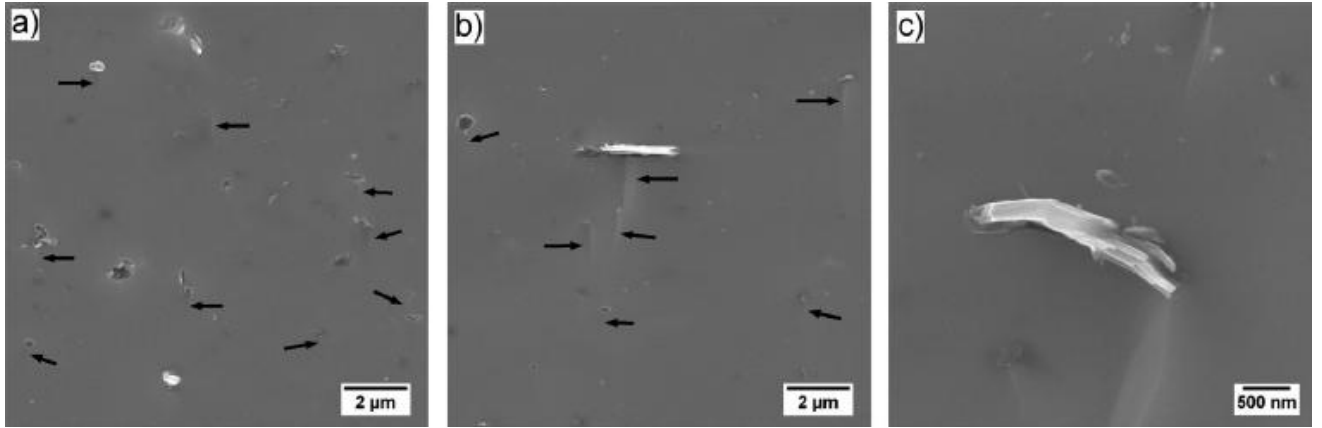
Fig. 7.5: SEM images for fracture surfaces showing pull-out of BNNTs, left behind cavities and the crack deflection around BNNTs (shown by arrows) in BS glass matrix reinforced by; a) 2.5 wt% BNNT-B; b) 2.5 wt% BNNT-C and; c) bundled up BNNT in BS glass matrix

7.1.4. Single Pass Scratch Resistance For the Composites

BS glass reinforced with 2.5 wt% and 5 wt% of BNNT-C type composites were tested to investigate the single pass scratch resistance of the composite samples compared to pure BS glass. The results of all the tested samples are given in Table 7.5. The scratch grooves were studied using confocal microscope and the observation is shown in Fig. 7.6.

The coefficient of friction (COF) of the sample increased slightly. Other important parameters like indenter displacement, normal and frictional forces were determined by the optical observation of scratch grooves, the profile (depth) of the scratch groove and the transition area measured by acoustic emission (AE) signalling.

Fig. 7.6(a-c) depicts the transition of micro-ductile (region I) to micro-cracking regime (region II) for pure glass as well as BNNT reinforced composites. It is clearly seen that the transition for composites occurred at longer indenter distance corresponding to higher normal and frictional loads compared to pure BS glass. The transition distances for composites were significantly higher than pure BS glass, i.e. ~0.28 mm for BS-2.5 wt% BNNT, ~0.30 mm for BS-5 wt% BNNT and ~0.23 mm for pure BS glass. The corresponding normal loads showed an increase of ~26% of scratch resistance for amorphous BS glass by addition of 5 wt% of BNNT (from ~268 mN for pure BS glass to ~337 nM for BS-5 wt% BNNT composite). In the scratch grooves observed for the samples by SEM, region I depicts the permanent plastic groove region. Fig. 7.6(a-b) show the plastic sub surface cracking under the scratch plastic region for pure BS and BS-2.5 wt% BNNT whereas no such feature is observed for BS-5 wt% BNNT. These sub surface lateral cracking, shown in Fig. 7.6(a), are commonly observed phenomena observed for amorphous glass scratches[97]. The region II is associated with the combination of lateral and radial cracking generated during Vickers indenter displacement above a critical load for a material, which leads to the chipping.

The radial cracks are common feature for micro-cracking regime found perpendicular to the direction of scratch displacement and their presence and intersection is shown in Fig. 7.6. (d) by dashed arrows. The combination of radial and

26

lateral cracks, lead to removal of material and hence we observed chipping of the samples which was a repeated process for the whole micro-cracking region and no other damages were observed for the samples. Extensive chipping and longer lateral cracks lead to severe damage to pure BS glass in comparison to the composites prepared. The overall scratch groove for BNNT reinforced BS glass was much smoother in comparison to pure BS glass. This study clearly indicated that introduction of BNNTs significantly improved the scratch resistance of BS glass compared to pure glass matrix.

Table 7.5: Scratch resistance for Pure BS and BS glass reinforced with 2.5 wt% BNNT and 5 wt% BNNT showing coefficient of friction (COF), transition displacement from micro-ductile to micro-cracking region, the lateral frictional force and normal force applied by the indenter on the surface

Material	COF	Transition (mm)	Friction force F_x (mN)	Normal force F_z (mN)
BS Pure	0.264 ± 0.038	0.234 ± 0.015	59 ± 2.1	268 ± 5
BS + 2.5 wt% BNNT-C	0.279 ± 0.033	0.281 ± 0.023	77.6 ± 3.3	323 ± 4
BS + 5 wt% BNNT-C	0.276 ± 0.031	0.297 ± 0.024	80.7 ± 2.9	337 ± 7
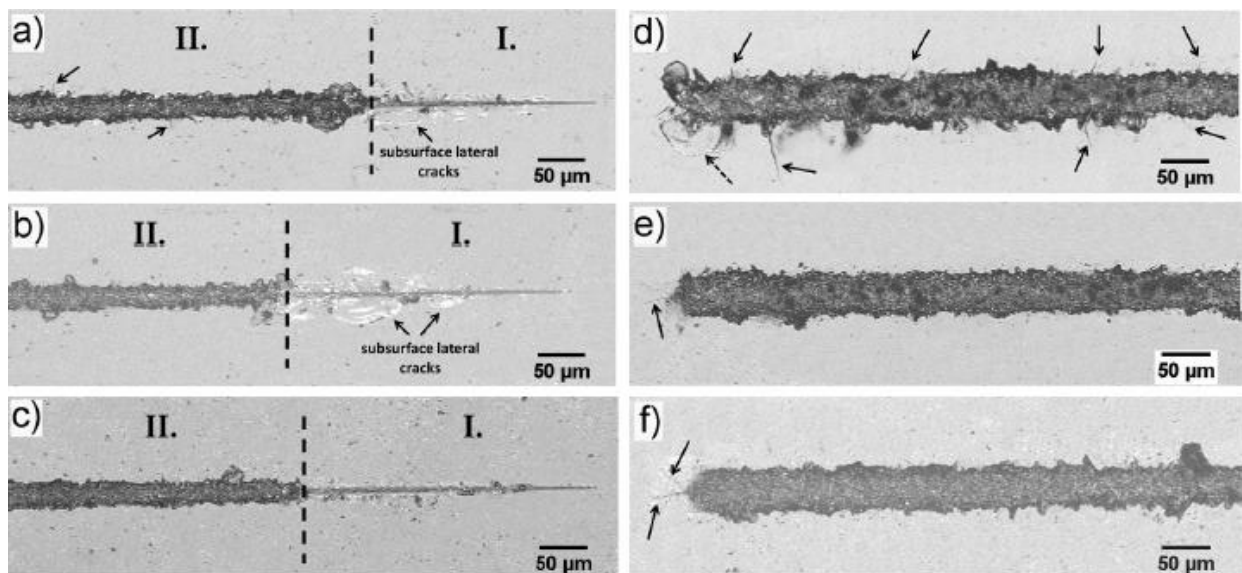
Fig. 7.6: Transition of scratch groove from micro-ductile to micro-cracking regime for a) pure BS glass, b) BS – 2.5 wt% BNNT-C, c) BS – 2.5 wt% BNNT-C. The scratch groove appearance on termination (at maximum load) for d) pure BS glass, e) BS – 2.5 wt% BNNT-C, f) BS – 2.5 wt% BNNT-C

7.2. BS-BNNS Composite

7.2.1. Material Analysis

The density of the boron nitride nanosheets were measured using helium pycnometer. After accounting the average of 20 values of measured densities, the density of BNNSs achieved was 1.8866 ± 0.0094 g/cm³. TGA of the BNNSs revealed that the BNNSs were found to be thermally stable until 650 °C after which the oxidation of BNNS takes place in ambient atmosphere.
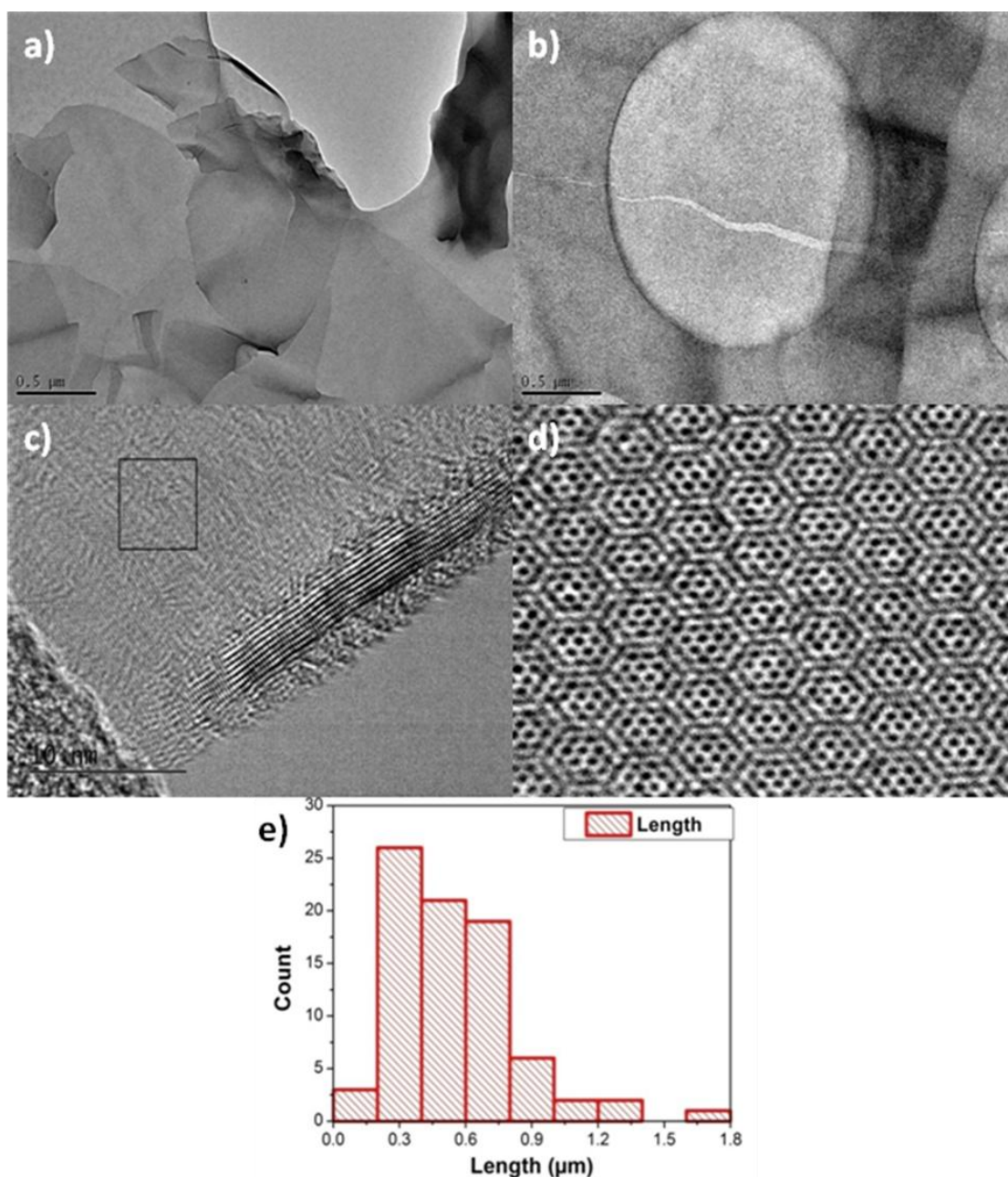
Fig. 7.7: (a) Low magnification TEM images of BNNSs; (b) Cracks observed in the BNNSs; (c) HRTEM showing fringes denoting curled BNNSs at edges; (d) Moiré patterns observed in BNNSs; (e) Statistic analysis of BNNSs along their length (longest dimension)

Zeta-potential for BNNS in ethanol was measured to be -18.8 mV. It should be noted that the charge measured on the pure BS powder in ethanol was -21.3 mV which confirms ethanol as a suitable solvent promoting deagglomeration of BNNSs in the composite.

The HRTEM images of the produced BNNSs prepared by liquid exfoliation technique are presented in Fig. 7.7(a) showing the boron nitride nanosheets formed due to shearing of the bulk h-BN powder. Cracks in the BNNSs presented in Fig. 7.7(b), were

28

commonly found, which might be the reason for breaking of larger BNNS to smaller ones. Fringes pattern developed in BNNSs due to the curved edges of the stacked BNNSs (Fig. 7.7(c)), with the spacing distance between the fringes of 0.33 nm to 0.37 nm, helped to deduce that the thickness of the BNNSs was between 4-30 layers. In Fig. 7.7(d) shows the Moiré pattern generated between the two stacking layers of BNNSs due to rotational orientation mismatch of 12.5°. The length of the BNNSs was statistically analyzed by calculating an average of 100 different sheets shown in Fig. 7.7(e) with an average size of 0.55 ± 0.29 μm along the longest dimension.
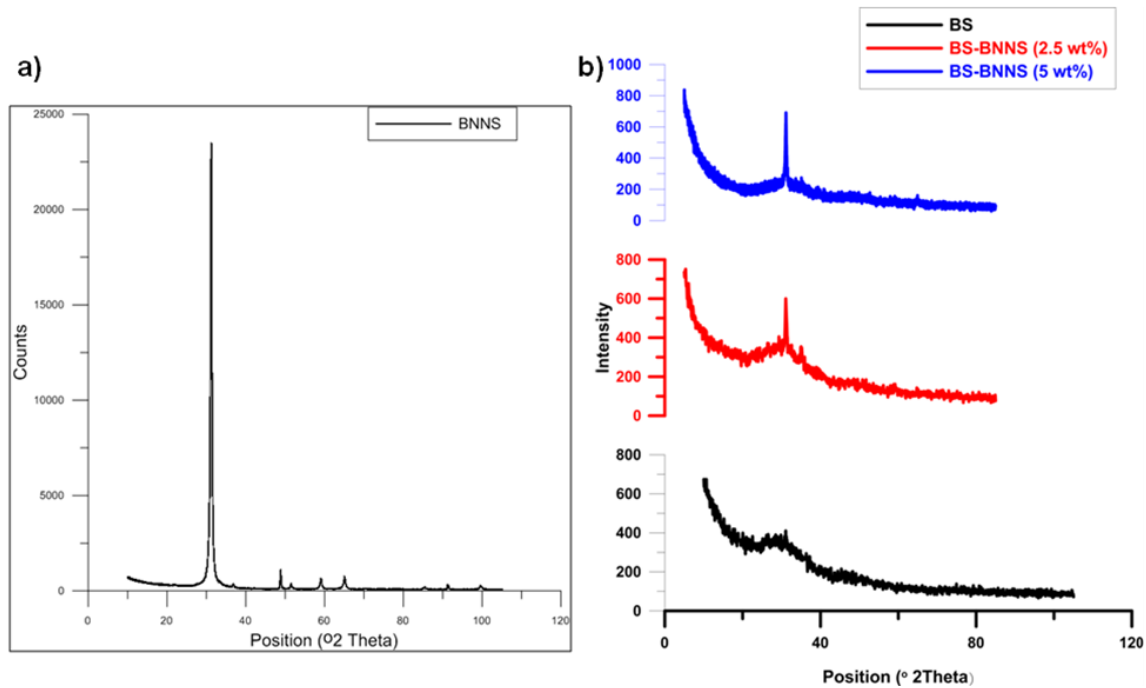
Fig. 7.8: XRD analysis of a) as produced BNNSs; b) BS and BNNSs reinforced BS with 2.5 wt% and 5 wt% concentration

XRD of the BNNSs revealed that they were highly crystalline with ~99% pure phase. The peak for BNNSs at was detected at 31.1° (Fig. 7.8(a)). XRD for BS - BNNS composites with BNNSs concentration of 0 wt%, 2.5 wt% and 5 wt% (Fig. 7.8(b)) was completely amorphous except for crystalline peak of BNNSs at 2 theta value of 31.1° whose intensity increased with the increasing concentration of BNNSs in BS glass matrix.

7.2.2. Microstructure Analysis

The relative densities of the bulk samples were measured using Archimedes principle and were calculated according to the rule of mixture. The relative densities of the pure BS, BS-BNNS (2.5 wt%) and BS-BNNS (5 wt%) are presented in Table 7.6. High densities also justify uniform dispersion of BNNSs in the composite.

Table 7.6: Relative densities and Young's modulus of pure BS, BS-BNNS (2.5 wt%) and BS-BNNS (5 wt%) composites

Material	Relative density (%)	Young's modulus (GPa)
BS	98.50	71.9 ± 0.7
BS-BNNS (2.5 wt%)	98.78	74.0 ± 1.5
BS-BNNS (5 wt%)	98.80	73.3 ± 3.0

Table 7.6. also depicts the Young's modulus for BS as well as BS-BNNS composites. The change observed in the Young's modulus of the nanocomposites compared to BS glass was not significant. This might be due to high bonding strength between BS and BNNSs making the composites behave as pure glass until the glass approached peak load at which de-cohesion between the interface of BNNSs and BS takes place.

7.2.3. Mechanical Properties

The fracture toughness of pure BS glass sample and BNNSs reinforced BS glass (0 wt%, 2.5 wt%, 5 wt%) was measured using chevron notch technique is presented in Table 7.7. below. Nearly 45% increase in the fracture toughness for the BS composite samples with reinforcement concentration of 5 wt% of BNNSs was observed. Similarly, flexural strength showed an increase of 45% in the flexural strength by reinforcing 5 wt% of BNNSs in BS matrix, are presented in Table 7.7. Here, it should be noted that the use of 5 wt% of BNNT increased the fracture toughness of BS glass by ~30%.

Table 7.7: Fracture toughness and flexural strength of BNNSs reinforced BS glass composite

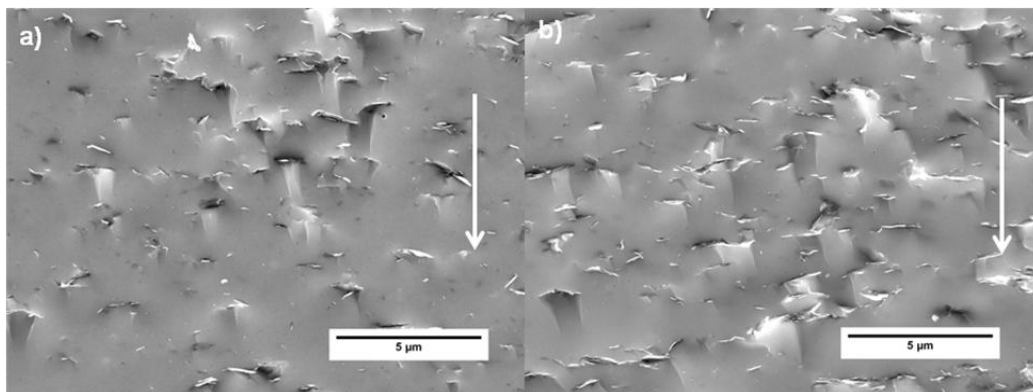| Sample	Fracture toughness (K_{IC})/MPa.m$^{1/2}$	Flexural Strength (σ_f)/MPa
BS	0.76 ± 0.05	82.2 ± 8.5
BS-BNNS (2.5 wt%)	1.01 ± 0.23	112.0 ± 13.8
BS-BNNS (5 wt%)	1.10 ± 0.11	119.0 ± 4.3

Fig. 7.9: Dispersion of BNNSs in BS for a) BS-BNNS (2.5 wt%); b) BS-BNNS (5 wt%) (arrows depicting applied force during fracture toughness measurement)

The dispersions of BNNSs in fracture surfaces of the broken specimens, as observed by SEM, were found to be uniformly dispersed and perpendicular to direction of sintering of the specimens in all three concentrations of BNNSs reinforced composites. The dispersions can be seen in Fig. 7.9. The white arrows show the direction of applied stress during sintering of the specimens as well as direction of applied force for the measurement of fracture toughness.

Fig. 7.10. shows the toughening mechanisms observed in BS-BNNS composite matrices. Fig. 7.10(a) shows the pull-out of stacked layer of BNNSs from the matrix due to applied stress and energy was utilized for breaking the bonding as well as dissipated energy overcoming frictional force[60] between the matrix and the BNNSs. Fig. 7.10(b) shows the crack behaviour observed in the pure BS glass which was relatively a straight path while Fig. 7.10(c) depicts the crack deflection observed in BS-BNNS (2.5 wt%) composite. The coefficient of thermal expansion (CTE) of the BN is negative (-2.9×10^{-6} K^{-1} at 293 K along a axis)[98] while the CTE of the BS is 3.3×10^{-6} K^{-1}. CTE for BNNSs and BS indicate that during the cooling process, the BNNSs expanded while the BS matrix shrank forming hoop compression stress on the expanding BNNSs in the matrix. Therefore, when the crack interacts with the BNNSs embedded, it is forced to deflect from its path around the 2D surface of BNNSs (Fig. 7.10(c)).
Fig. 7.10(d) shows the crack bridging observed in BS-BNNS (5 wt%) composite during which the crack encountered BNNSs embedded in the matrix, which anchored the matrix and acted as a bridge, delaying the further opening of the crack.
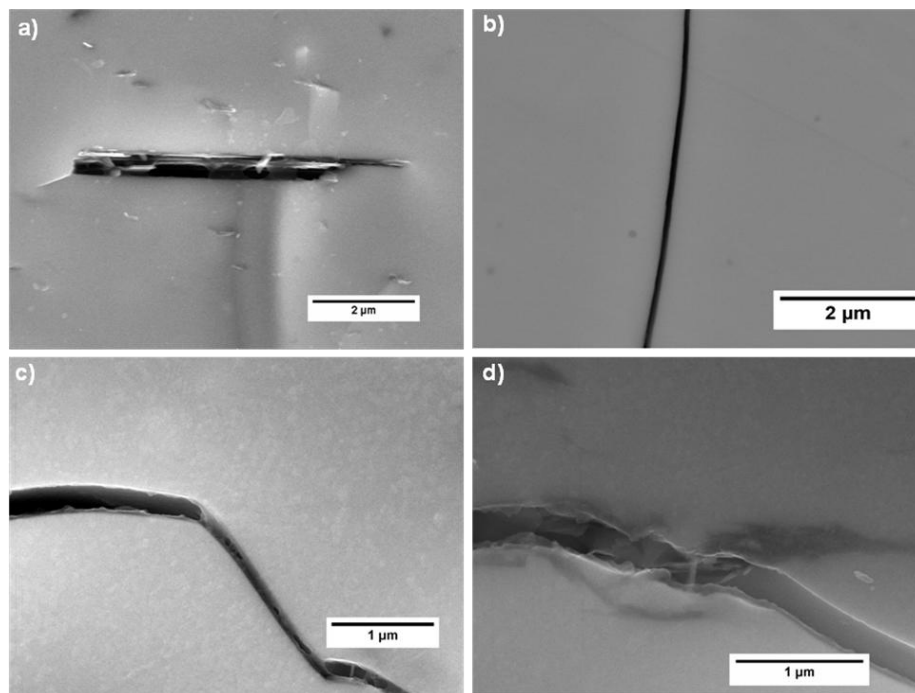

Fig. 7.10: Toughening mechanisms observed in BNNSs reinforced BS matrix a) Pull-out of inner layers of stack of BNNSs from BS matrix; b) straight crack in pure BS matrix; c) crack deflection observed in BS-BNNS (2.5 wt%) composite; d) crack bridging observed in BS-BNNS (5 wt%) composite

Increase in the flexural strength of the composites might be observed due to effective transfer of elastic energy gained by the BS matrix to BNNSs embedded in the matrix because of favourable interfacial bonding between them[30, 33].

7.2.4. Wear Properties

The wear tests for 2.5 wt% BNNSs and 5 wt% BNNSs were conducted using BS and alumina balls. The Coefficient of Friction (COF), wear rate and normalized wear resistance are presented in Table 7.8. for the tribology tests performed by BS glass ball. It can be seen that with the increasing concentration of BNNSs up till 5%, the average COF decreases by 23 % for a sliding distance of 500 m which may be due to BNNSs acting as a lubricating surfaces for the composites thereby reducing friction on the surface during sliding.

Table 7.8: Values of COF, wear rate and wear resistance for Pure BS, BS-BNNS (2.5 wt%) and BS-BNNS (5 wt%) measured by tribological tests using BS ball

Sample	COF	Wear rate (mm^3/Nm)	Normalized wear resistance
BS	0.78 ± 0.16	12.95×10^{-4}	1
BS-BNNS(2.5 wt%)	0.83 ± 0.14	8.82×10^{-4}	1.47
BS-BNNS (5 wt%)	0.60 ± 0.09	4.93×10^{-4}	2.63

The wear rates were measured after the completion of tests. There was a linear drop in the wear rate (as shown in Fig. 7.11. (a)) with the increasing concentration of BNNSs in the composite signifying the effective role of BNNSs in the matrix. The wear resistance of the composites showed a marked increase of ~2.6 times by the introduction of 5 wt% of BNNSs. This may be because of higher concentration of BNNSs forming well connected network of BNNSs in the composites providing higher lubrication on the surface which aided in sliding and limiting friction[11],[68]. The dramatic increase in the wear resistance could also be linked to the improved mechanical properties which were observed for BS-BNNS composites.

The hardness of the alumina ball is much higher than of BS ball as well as the BS matrix used in the composite, therefore, very low wear was observed the alumina ball after the completion of wear tests through alumina ball. It may be due to this reason, a negligible change in the COF of the composite with 5 wt% of BNNSs and high wear rate was observed[70],[11],[55] compared to pure BS glass.
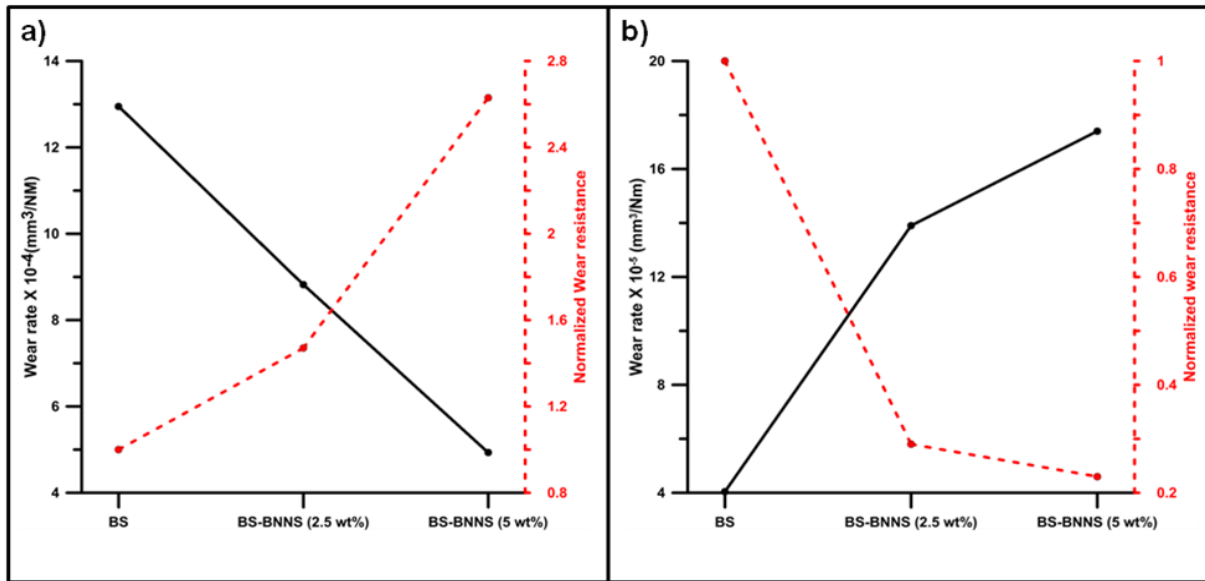
Fig. 7.14: Wear rate (black solid line) and wear resistance (red dashed line) for BS, BS-BNNS (2.5 wt%) and BS-BNNS (5 wt%) measured with; (a) BS ball; (b) alumina ball

7.3. Comparative Analysis

7.3.1. Comparison of the Effect of BNNS and BNNT as Reinforcements in BS Matrix

The BNNS offer better improvement in fracture toughness of BS glass (~45%) in comparison to increase offered by BNNTs (~30%) with 5 wt% concentration. Even the use of different morphologies of BNNTs, i.e. bamboo type and cylindrical shape, also did not contribute to any significant change in these properties.

The role of these reinforcements in the brittle matrices was to increase the toughness of the material so that the failure of the material was delayed in comparison to general catastrophic failure experienced in the pure glass matrix. As explained in earlier sections, although the properties of the reinforcements are important, the interface between the reinforcement and the matrix plays a major role in determining the mechanical properties of the composites. The role of BNNS as a mechanical reinforcement was more pronounced in comparison to the BNNTs because of several factors as follows.

7.3.1.1. Surface Morphology

The BNNS possess comparatively rougher and uneven morphology of the surface compared to the BNNTs due to presence of higher defect density on the surface of BNNSs created during high energy shearing during the synthesis of BNNS. The uneven surface helped in better interlocking of BNNS and BS matrix at the interface during sintering process compared to comparatively smoother surface morphology of the BNNTs which helped in efficient load transfer from the matrix to reinforcement thereby improving the toughness of BS matrix.

33

7.3.1.2. Higher Surface Area

BNNS ($\sim$927 m^2/g) [66] possess larger surface area in comparison to BNNT (200-300 m^2/g) [67]. The advantage of higher value of surface area for BNNS was that it provides larger contact surface available to the matrix due to 2D structure (sheet structure). It contributed to the better load transfer from the matrix to the BNNS improving the toughening of the matrix.

7.3.1.3. Geometrical Benefits

BNNSs having 2D geometry possess added advantage as compared to 1D geometry of the BNNTs. When the micro-crack propagation came in contact with the BNNSs, the toughening mechanisms were encountered in two dimensions around the nanosheets, i.e. along length and breadth (thickness dimension in nm). Crack deflection is the most effective toughening mechanism which is advantageous and responsible for higher values to fracture toughness for BNNS.

7.3.1.4. Agglomeration

Nano reinforcements suffer from a severe drawback of agglomeration due to high surface energy and they cannot be utilized to full potential if they suffer from agglomeration therefore well dispersed phases of nano reinforcement are required. Geometrically, owing to the 2D structure, the BNNSs have far lesser tendency to agglomerate in comparison to BNNTs thereby improving the properties of BNNSs reinforced composite more than that of BNNTs reinforced glass.

Other than the above mentioned properties, the use of BNNSs as reinforcements is more cost effective as preparation of high quality BNNSs can be carried out by far more convenient methods compared to BNNT. BNNSs preparation methods also provide quantitatively much better final yield after preparation compared to BNNTs. Other than complicated fabrication methods, BNNTs have to be functionalized in order to prevent agglomeration though due to inert nature of BNNT, it is a difficult task. Therefore, use of BNNSs as reinforcements appears to be more beneficial compared to BNNTs.

8. Conclusion

In the present work, various issues dealing with preparation and processing of BNNT and BNNS reinforced BS glass composites were investigated as well as optimized to achieve the best results. These composites were characterized for their microstructural, mechanical and tribological properties. The effects of reinforcing different geometries of BN nanomaterial were studied. Interestingly, 1D (BNNT) and 2D (BNNS) geometry of BN materials showed different results despite having same/similar functional properties.

8.1. BNNT and BNNT Reinforced BS Glass Composites

BNNT with two morphologies, i.e. cylindrical type and bamboo like were used to reinforce amorphous BS glass with concentration 0 wt%, 2.5 wt% and 5 wt%. The present results clearly signify that increasing concentration of BNNT directly influenced the properties of BNNT reinforced BS composites.   The as-received tandard quality BNNT did not improve the mechanical properties of bulk composites due to presence of small pores throughout the surface due to Fe impurities present in the BNNTs. Successful purification of BNNTs was carried out to remove the Fe impurities by acid washing leading to reduction of Fe impurities from ∼54 wt% down to 1 wt%. The main results are summarized as follows:

1. Well dispersed and highly dense BNNT-BS glass matrix composites were prepared using powder processing routes achieving a density of ∼98% by reinforcing 5 wt% of BNNTs.
2. A unimportant decrease of ∼7% was observed in the hardness and Young's modulus of the 5 wt% reinforced BNNTs composites compared to pure BS glass due to decrease in relative density.
3. The fracture toughness measured by Vickers indentation method and by chevron notched beam was quite similar showed an increase of ∼30% for 5 wt% purified BNNT reinforcement compared to pure glass.
4. Pull-out, crack bridging, BNNT stretching and crack deflection were the main toughening mechanisms observed for prepared composite materials.
5. Stretching of entangled BNNTs was uniquely observed as a strong toughening mechanism the matrix where the entangled BNNT were anchored on both edges of the crack opening ultimately leading to lesser opening width of the crack.
6. Sword-in-sheath mechanism was observed for BNNTs and the outer layer of the multiwalled nanotubes had a strong bonding interface with the matrix.
7. Efficient load transfer from the matrix to the BNNTs was observed leading to enhancement in fracture toughness of the glass composites.
8. Improvement in the scratch resistance (∼26%) was observed for glass composites by incorporating ∼5 wt% of BNNT in BS glass.

8.2. BNNS and BNNS Reinforced BS Glass Composites

1. BNNSs were successfully prepared using liquid exfoliation technique by delamination of the BNNS from the defect site producing BNNSs with the longest dimension of ~0.55 ± 0.29 μm.

2. BNNSs prepared were highly crystalline and the oxidation temperature for the BNNSs was ~650°C.

3. These BNNSs were used as reinforcement for BS glass and the well dispersed BNNSs based composites were prepared by powder processing and consolidated by spark plasma sintering with the concentrations of loading of BNNS as 0 wt%, 2.5 wt% and 5 wt%.

4. The density of the samples under the specific SPS conditions applied observed was quite high (i.e. > 98.5%) even after reinforcing 5 wt% of BNNS signifying limited agglomeration in the BNNSs dispersed in the matrix and the composite samples were observed to be completely amorphous except for the crystalline peak of BNNS observed.

5. No or negligible change in Young's modulus of the composite samples was observed in comparison to the pure BS glass.

6. Improvement in the fracture toughness by ~45% each for 5 wt% of BNNS reinforced BS composite (1.10 MPa.m$^{1/2}$) was observed in comparison to pure glass (0.76 MPa.m$^{1/2}$).

7. Toughening mechanisms like pull-out, crack bridging and crack deflection were the main observed for the characterized composite materials. The BNNSs were observed to be aligned perpendicular to the direction of applied force during sintering and uniformly dispersed throughout the matrix.

8. Improvement in the flexural strength by ~45% each for 5 wt% of BNNS reinforced BS composite (~119 MPa) was observed in comparison to pure glass (~82 MPa).

9. Good interfacial bonding for BNNS and BS glass matrix was observed leading to efficient load transfer.

10. Improved tribological properties of the BNNS reinforced BS glass composites were observed by using BS glass ball as a counterpart. A reduction of ~23% of coefficient of friction was observed by incorporating 5 wt% of BNNS in BS glass.

11. The wear rate drops linearly by using BS ball as a counterpart with increasing concentration of BNNS from 0 wt% to 5 wt%.

Therefore, on the basis of presented results, 2D nanomaterials (BNNSs) act as more efficient mechanical reinforcement compared to 1D nanomaterials (BNNTs).

References

1. Weiner, S.; Wagner, H. D., The material bone: Structure mechanical function relations. *Annual Review of Materials Science* **1998,** *28*, 271-298.
2. Park, S.; Seo, M. K., *Interface Science and Composites*. Elsevier Academic Press: **2011**.
3. Koichi, N., New design concept of structural ceramics—Ceramic nanocomposites. *The Centennial Memorial Issue of The Ceramic Society of Japan* **1991,** *99* (10), 974-982.
4. Cho, J.; Inam, F.; Reece, M. J.; Chlup, Z.; Dlouhy, I.; Shaffer, M. S. P.; Boccaccini, A. R., Carbon nanotubes: do they toughen brittle matrices? *Journal of Materials Science* **2011,** *46* (14), 4770-4779.
5. Bansal, N. P.; Hurst, J. B.; Choi, S. R., Boron Nitride Nanotubes-Reinforced Glass Composites. *Journal of the American Ceramic Society* **2006,** *89* (1), 388-390.
6. Bernardo, E.; Nicolais, L., Glass Matrix Composite. In *Wiley Encyclopedia of Composites*, John Wiley & Sons, Inc.: **2011**.
7. Donald, I. W. In *Preparation, properties and applications of glass and glass-ceramic matrix composites*, **1995**; Trans Tech Publ: pp 123-144.
8. Fibre reinforcements. In *Fundamentals of Fibre Reinforced Composite Materials*, Taylor & Francis: **2005**; pp 19-81.
9. Brennan, J. J.; Nutt, S. R., SiC-Whisker-Reinforced Glass-Ceramic Composites: Interfaces and Properties. *Journal of the American Ceramic Society* **1992,** *75* (5), 1205-1216.
10. Moya, J. S., Layered ceramics. *Advanced Materials* **1995,** *7* (2), 185-189.
11. Porwal, H.; Tatarko, P.; Grasso, S.; Hu, C.; Boccaccini, A. R.; Dlouhy, I.; Reece, M. J., Toughened and machinable glass matrix composites reinforced with graphene and graphene-oxide nano platelets. *Science and Technology of Advanced Materials* **2013,** *14* (5).
12. Boccaccini, A. R., Glass and Glass-Ceramic Matrix Composite Materials. *Journal of the Ceramic Society of Japan* **2001,** *109* (1271), S99-S109.
13. Evans A. G., Zok F. W., Review The physics and mechanics of fibre-reinforced brittle matrix composites. *Journal of materials science* **1994,** (29), 3857-3896.
14. Dlouhý, I.; Chlup, Z.; Atiq, S.; Boccaccini, A. R., Fracture Resistance of Hybrid Glass Matrix Composite and Its Degradation Due to Thermal Ageing and Thermal Shock. In *Fracture Mechanics of Ceramics: Active Materials, Nanoscale Materials, Composites, Glass and Fundamentals*, Bradt, R. C.; Munz, D.; Sakai, M.; White, K. W., Eds. Springer US: Boston, MA, **2005**; pp 263-274.
15. Chawla, N.; Chawla, K. K.; Koopman, M.; Patel, B.; Coffin, C.; Eldridge, J. I., Thermal-shock behavior of a Nicalon-fiber-reinforced hybrid glass-ceramic composite. *Composites Science and Technology* **2001,** *61* (13), 1923-1930.
16. Sambell R. A. J., B. A., Phillips D. C., Bowen D.H., Carbon fibre composites with ceramic and glass matrices *Journal of Materials Science* **1972,** (7), 676-681.
17. Rouxel, T.; Lavelle, C.; Garnier, C.; Verdier, P.; Laurent, Y., Mechanical evaluation of SiC particle reinforced oxynitride glass and glass-ceramic composites. *Scripta Metallurgica et Materialia* **1994,** *31* (1), 15-20.
18. Hasselman, D. P. H.; Zdaniewski, W. A.; Swearengen, J. C.; Beauchamp, E. K., Effect of alumina dispersions on the thermal conductivity/diffusivity and thermal stress resistance of a borosilicate glass. *Journal of Materials Science* **1980,** *15* (2), 518-520.
19. Rawlings, R. D., Glass-ceramic matrix composites. *Composites* **1994,** *25* (5), 372-379.
20. Zhang, X.; Wang, Y.; Lu, J.; Zang, J.; Zhang, J.; Ge, E., Wettability and reactivity in diamond–borosilicate glass system. *International Journal of Refractory Metals and Hard Materials* **2010,** *28* (2), 260-264.

21. Skorokhod, V. V., Layered Composites: Structural Classification, Thermophysical and Mechanical Properties. *Powder Metallurgy and Metal Ceramics* **2003,** *42* (9), 437-446.

22. Bansal, N. P., *Handbook of ceramic composites*. Springer: **2006**; Vol. 200.

23. Bangali, J.; Rane, S.; Phatak, G.; Gangal, S., Effect of ink organics on cambering of an Ag-metallized low temperature co-fired ceramics (LTCC). *Journal of Materials Science: Materials in Electronics* **2008,** *20* (5), 455-460.

24. Alias, R., 24 - Multilayer glass–ceramic composites for microelectronics: processing and properties A2 - Low, I.M. In *Advances in Ceramic Matrix Composites*, Woodhead Publishing: **2014**; pp 587-610.

25. Leighton, K.; Carberry, J.; Serafin, W.; Avery, T.; Templeton, D., Transparent Armor for the New Standard in Battlefield Performance. In *Advances in Ceramic Armor VII*, John Wiley & Sons, Inc.: **2011**; pp 27-41.

26. Gao, F., Clay/polymer composites: the story. *Materials Today* **2004,** *7* (11), 50-55.

27. Mark, J. E., Ceramic-reinforced polymers and polymer-modified ceramics. *Polymer Engineering & Science* **1996,** *36* (24), 2905-2920.

28. Wen, J.; Wilkes, G. L., Organic/Inorganic Hybrid Network Materials by the Sol−Gel Approach. *Chemistry of Materials* **1996,** *8* (8), 1667-1681.

29. Scotti, R.; Conzatti, L.; D'Arienzo, M.; Di Credico, B.; Giannini, L.; Hanel, T.; Stagnaro, P.; Susanna, A.; Tadiello, L.; Morazzoni, F., Shape controlled spherical (0D) and rod-like (1D) silica nanoparticles in silica/styrene butadiene rubber nanocomposites: Role of the particle morphology on the filler reinforcing effect. *Polymer* **2014,** *55* (6), 1497-1506.

30. Mukhopadhyay, A.; Chu, B. T. T.; Green, M. L. H.; Todd, R. I., Understanding the mechanical reinforcement of uniformly dispersed multiwalled carbon nanotubes in alumino-borosilicate glass ceramic. *Acta Materialia* **2010,** *58* (7), 2685-2697.

31. Fan, J.; Zhao, D.; Wu, M.; Xu, Z.; Song, J., Preparation and Microstructure of Multi-Wall Carbon Nanotubes-Toughened Al_2O_3 Composite. *Journal of the American Ceramic Society* **2006,** *89* (2), 750-753.

32. Michalek, M.; Bodisova, K.; Michalkova, M.; Sedlacek, J.; Galusek, D., Alumina/MWCNTs composites by aqueous slip casting and pressureless sintering. *Ceramics International* **2013,** *39* (6), 6543-6550.

33. Ye, F.; Liu, L.; Wang, Y.; Zhou, Y.; Peng, B.; Meng, Q., Preparation and mechanical properties of carbon nanotube reinforced barium aluminosilicate glass-ceramic composites. *Scripta Materialia* **2006,** *55* (10), 911-914.

34. Mazaheri, M.; Mari, D.; Hesabi, Z. R.; Schaller, R.; Fantozzi, G., Multi-walled carbon nanotube/nanostructured zirconia composites: Outstanding mechanical properties in a wide range of temperature. *Composites Science and Technology* **2011,** *71* (7), 939-945.

35. Chopra, N. G.; Luyken, R. J.; Cherrey, K.; Crespi, V. H.; Cohen, M. L.; Louie, S. G.; Zettl, A., Boron nitride nanotubes. *Science* **1995,** *269* (5226), 966-7.

36. Paine, R. T.; Narula, C. K., Synthetic routes to boron nitride. *Chemical Reviews* **1990,** *90* (1), 73-91.

37. Ishii, T.; Sato, T.; Sekikawa, Y.; Iwata, M., Growth of whiskers of hexagonal boron nitride. *Journal of Crystal Growth* **1981,** *52*, 285-289.

38. Golberg, D.; Bando, Y.; Tang, C.; Zhi, C., Boron nitride nanotubes. *Advanced Materials* **2007,** *19* (18), 2413-2432.

39. Golberg, D.; Bando, Y.; Huang, Y.; Terao, T.; Mitome, M.; Tang, C.; Zhi, C., Boron Nitride Nanotubes and Nanosheets. *Acs Nano* **2010,** *4* (6), 2979-2993.

40. Cohen, X. B. a. A. R. a. S. G. L. a. M. L., Stability and Band Gap Constancy of Boron Nitride Nanotubes. *EPL (Europhysics Letters)* **1994,** *28* (5), 335.

41. Verma, V.; Jindal, V. K.; Dharamvir, K., Elastic moduli of a boron nitride nanotube. *Nanotechnology* **2007,** *18* (43).

42. Suryavanshi, A. P.; Yu, M. F.; Wen, J. G.; Tang, C. C.; Bando, Y., Elastic modulus and resonance behavior of boron nitride nanotubes. *Applied Physics Letters* **2004,** *84* (14), 2527-2529.

43. Bettinger, H. F.; Dumitrica, T.; Scuseria, G. E.; Yakobson, B. I., Mechanically induced defects and strength of BN nanotubes. *Physical Review B* **2002,** *65* (4).

44. Boubakeur Essedik Belkerk and Amine Achour and Dongyan Zhang and Salah Sahli and, M. A. D. a. Y. K. Y., Thermal conductivity of vertically aligned boron nitride nanotubes. *Applied Physics Express* **2016,** *9* (7), 075002.

45. Chang, C. W.; Fennimore, A. M.; Afanasiev, A.; Okawa, D.; Ikuno, T.; Garcia, H.; Li, D.; Majumdar, A.; Zettl, A., Isotope Effect on the Thermal Conductivity of Boron Nitride Nanotubes. *Physical Review Letters* **2006,** *97* (8), 085901.

46. Wei, X.; Wang, M.-S.; Bando, Y.; Golberg, D., Tensile Tests on Individual Multi-Walled Boron Nitride Nanotubes. *Advanced Materials* **2010,** *22* (43), 4895-4899.

47. Du, M.; Bi, J.-Q.; Wang, W.-L.; Sun, X.-L.; Long, N.-N., Microstructure and properties of SiO2 matrix reinforced by BN nanotubes and nanoparticles. *Journal of Alloys and Compounds* **2011,** *509* (41), 9996-10002.

48. Nigues, A.; Siria, A.; Vincent, P.; Poncharal, P.; Bocquet, L., Ultrahigh interlayer friction in multiwalled boron nitride nanotubes. *Nature Materials* **2014,** *13* (7), 688-693.

49. Lahiri, D.; Hadjikhani, A.; Zhang, C.; Xing, T.; Li, L. H.; Chen, Y.; Agarwal, A., Boron nitride nanotubes reinforced aluminum composites prepared by spark plasma sintering: Microstructure, mechanical properties and deformation behavior. *Materials Science and Engineering a-Structural Materials Properties Microstructure and Processing* **2013,** *574*, 149-156.

50. Wang, X.-B.; Weng, Q.; Wang, X.; Li, X.; Zhang, J.; Liu, F.; Jiang, X.-F.; Guo, H.; Xu, N.; Golberg, D.; Bando, Y., Biomass-Directed Synthesis of 20 g High-Quality Boron Nitride Nanosheets for Thermoconductive Polymeric Composites. *Acs Nano* **2014,** *8* (9), 9081-9088.

51. Zhi, C. Y.; Bando, Y.; Wang, W. L.; Tang, C. C.; Kuwahara, H.; Golberg, D., Mechanical and Thermal Properties of Polymethyl Methacrylate-BN Nanotube Composites. *Journal of Nanomaterials* **2008**.

52. Lahiri, D.; Singh, V.; Benaduce, A. P.; Seal, S.; Kos, L.; Agarwal, A., Boron nitride nanotube reinforced hydroxyapatite composite: Mechanical and tribological performance and in-vitro biocompatibility to osteoblasts. *Journal of the Mechanical Behavior of Biomedical Materials* **2011,** *4* (1), 44-56.

53. Tatarko, P.; Grasso, S.; Porwal, H.; Chlup, Z.; Saggar, R.; Dlouhy, I.; Reece, M. J., Boron nitride nanotubes as a reinforcement for brittle matrices. *Journal of the European Ceramic Society* **2014,** *34* (14), 3339-3349.

54. Du, M.; Bi, J.-Q.; Wang, W.-L.; Sun, X.-L.; Long, N.-N., Influence of sintering temperature on microstructure and properties of SiO2 ceramic incorporated with boron nitride nanotubes. *Materials Science and Engineering a-Structural Materials Properties Microstructure and Processing* **2012,** *543*, 271-276.

55. Tatarko, P.; Grasso, S.; Chlup, Z.; Porwal, H.; Kasiarova, M.; Dlouhy, I.; Reece, M. J., Toughening effect of multi-walled boron nitride nanotubes and their influence on the sintering behaviour of 3Y-TZP zirconia ceramics. *Journal of the European Ceramic Society* **2014,** *34* (7), 1829-1843.

56. Yu, H.-H.; Wang, S.-R.; Yang, L.-Y., R-Curve Behavior of Si3N4/BNNT Composites. *Applied Composite Materials* **2013,** *20* (5), 947-960.

57. Xu, J.-J.; Bai, Y.-J.; Wang, W.-L.; Wang, S.-R.; Han, F.-D.; Qi, Y.-X.; Bi, J.-Q., Toughening and reinforcing zirconia ceramics by introducing boron nitride nanotubes. *Materials Science and Engineering a-Structural Materials Properties Microstructure and Processing* **2012,** *546*, 301-306.

58. Novoselov, K. S.; Geim, A. K.; Morozov, S. V.; Jiang, D.; Zhang, Y.; Dubonos, S. V.; Grigorieva, I. V.; Firsov, A. A., Electric field effect in atomically thin carbon films. *Science* **2004,** *306* (5696), 666-9.

59. Walker, L. S.; Marotto, V. R.; Rafiee, M. A.; Koratkar, N.; Corral, E. L., Toughening in Graphene Ceramic Composites. *ACS Nano* **2011,** *5* (4), 3182-3190.

60. Gao, C.; Liu, T.; Shuai, C.; Peng, S., Enhancement mechanisms of graphene in nano-58S bioactive glass scaffold: mechanical and biological performance. *Scientific Reports* **2014,** *4*.

61. Porwal, H.; Grasso, S.; Reece, M. J., Review of graphene-ceramic matrix composites. *Advances in Applied Ceramics* **2013,** *112* (8), 443-454.

62. Geim, A. K.; Novoselov, K. S., The rise of graphene. *Nat Mater* **2007,** *6* (3), 183-191.

63. Fan, Y.; Wang, L.; Li, J.; Li, J.; Sun, S.; Chen, F.; Chen, L.; Jiang, W., Preparation and electrical properties of graphene nanosheet/Al2O3 composites. *Carbon* **2010,** *48* (6), 1743-1749.

64. He, T.; Li, J.; Wang, L.; Zhu, J.; Jiang, W., Preparation and Consolidation of Alumina/Graphene Composite Powders. *MATERIALS TRANSACTIONS* **2009,** *50* (4), 749-751.

65. Lin, Y.; Connell, J. W., Advances in 2D boron nitride nanostructures: nanosheets, nanoribbons, nanomeshes, and hybrids with graphene. *Nanoscale* **2012,** *4* (22), 6908-6939.

66. Nag, A.; Raidongia, K.; Hembram, K. P. S. S.; Datta, R.; Waghmare, U. V.; Rao, C. N. R., Graphene Analogues of BN: Novel Synthesis and Properties. *Acs Nano* **2010,** *4* (3), 1539-1544.

67. Tiano, A. L.; Park, C.; Lee, J. W.; Luong, H. H.; Gibbons, L. J.; Chu, S.-H.; Applin, S. I.; Gnoffo, P.; Lowther, S.; Kim, H. J.; Danehy, P. M.; Inman, J. A.; Jones, S. B.; Kang, J. H.; Sauti, G.; Thibeault, S. A.; Yamakov, V.; Wise, K. E.; Su, J.; Fay, C. C. In *Boron Nitride Nanotube: Synthesis and Applications*, Conference on Nanosensors, Biosensors, and Info-Tech Sensors and Systems, San Diego, CA, **2014**

68. Lee, B.; Lee, D.; Lee, J. H.; Ryu, H. J.; Hong, S. H., Enhancement of toughness and wear resistance in boron nitride nanoplatelet (BNNP) reinforced Si3N4 nanocomposites. *Scientific Reports* **2016,** *6*, 27609.

69. Inam, F.; Yan, H.; Peijs, T.; Reece, M. J., The sintering and grain growth behaviour of ceramic–carbon nanotube nanocomposites. *Composites Science and Technology* **2010,** *70* (6), 947-952.

70. Porwal, H.; Tatarko, P.; Grasso, S.; Khaliq, J.; Dlouhy, I.; Reece, M. J., Graphene reinforced alumina nano-composites. *Carbon* **2013,** *64*, 359-369.

71. Porwal, H.; Kasiarova, M.; Tatarko, P.; Grasso, S.; Dusza, J.; Reece, M. J., Scratch behaviour of graphene alumina nanocomposites. *Advances in Applied Ceramics* **2015,** *114* (sup1), S34-S41.

72. Reed, J. S., *Principles of Ceramics Processing*. 2nd ed.; John Wiley & Sons: New York, **1995**.

73. George Y. Onoda , L. L. H., *Ceramic Processing before Firing*. John Wiley & Sons: New York, **1978**.

74. Wang, K.; Wang, Y.; Fan, Z.; Yan, J.; Wei, T., Preparation of graphene nanosheet/alumina composites by spark plasma sintering. *Materials Research Bulletin* **2011,** *46* (2), 315-318.

75. Dunn, B.; Zink, J. I., Molecules in glass: probes, ordered assemblies, and functional materials. *Acc Chem Res* **2007,** *40* (9), 747-55.

76. Zhou, J. C.; Chuang, M. H.; Lan, E. H.; Dunn, B.; Gillman, P. L.; Smith, S. M., Immunoassays for cortisol using antibody-doped sol-gel silica. *Journal of Materials Chemistry* **2004,** *14* (14), 2311-2316.

77. Lim, J.; Malati, P.; Bonet, F.; Dunn, B., Nanostructured Sol-Gel Electrodes for Biofuel Cells. *Journal of The Electrochemical Society* **2007,** *154* (2), A140-A145.

78. Watcharotone, S.; Dikin, D. A.; Stankovich, S.; Piner, R.; Jung, I.; Dommett, G. H. B.; Evmenenko, G.; Wu, S.-E.; Chen, S.-F.; Liu, C.-P.; Nguyen, S. T.; Ruoff, R. S., Graphene−Silica Composite Thin Films as Transparent Conductors. *Nano Letters* **2007,** *7* (7), 1888-1892.

79. Bechelany, M.; Bernard, S.; Brioude, A.; Cornu, D.; Stadelmann, P.; Charcosset, C.; Fiaty, K.; Miele, P., Synthesis of Boron Nitride Nanotubes by a Template-Assisted Polymer Thermolysis Process. *The Journal of Physical Chemistry C* **2007,** *111* (36), 13378-13384.

80. Ji, F.; Li, Y.-L.; Feng, J.-M.; Su, D.; Wen, Y.-Y.; Feng, Y.; Hou, F., Electrochemical performance of graphene nanosheets and ceramic composites as anodes for lithium batteries. *Journal of Materials Chemistry* **2009,** *19* (47), 9063-9067.

81. Walker, R. F., Mechanism of Material Transport During Sintering. *Journal of the American Ceramic Society* **1955,** *38* (6), 187-197.

82. Inam, F.; Yan, H.; Reece, M. J.; Peijs, T., Structural and chemical stability of multiwall carbon nanotubes in sintered ceramic nanocomposite. *Advances in Applied Ceramics* **2010,** *109* (4), 240-247.

83. Lin Hwang, G.; Chu Hwang, K., Carbon nanotube reinforced ceramics. *Journal of Materials Chemistry* **2001,** *11* (6), 1722-1725.

84. Chen, I. W.; Wang, X. H., Sintering dense nanocrystalline ceramics without final-stage grain growth. *Nature* **2000,** *404* (6774), 168-71.

85. Bodišová, K.; Galusek, D.; Švančárek, P.; Pouchlý, V.; Maca, K., Grain growth suppression in alumina via doping and two-step sintering. *Ceramics International* **2015,** *41* (9, Part B), 11975-11983.

86. Boccaccini, A. R.; Acevedo, D. R.; Brusatin, G.; Colombo, P., Borosilicate glass matrix composites containing multi-wall carbon nanotubes. *Journal of the European Ceramic Society* **2005,** *25* (9), 1515-1523.

87. Hu, C.; Li, F.; Qu, D.; Wang, Q.; Xie, R.; Zhang, H.; Peng, S.; Bao, Y.; Zhou, Y., 8 - Developments in hot pressing (HP) and hot isostatic pressing (HIP) of ceramic matrix composites A2 - Low, I.M. In *Advances in Ceramic Matrix Composites*, Woodhead Publishing: **2014**; pp 164-189.

88. Li, J.; Liao, H.; Hermansson, L., Sintering of partially-stabilized zirconia and partially-stabilized zirconia—hydroxyapatite composites by hot isostatic pressing and pressureless sintering. *Biomaterials* **1996,** *17* (18), 1787-1790.

89. Grasso, S.; Yoshida, H.; Porwal, H.; Sakka, Y.; Reece, M., Highly transparent α-alumina obtained by low cost high pressure SPS. *Ceramics International* **2013,** *39* (3), 3243-3248.

90. Centeno, A.; Rocha, V. G.; Alonso, B.; Fernández, A.; Gutierrez-Gonzalez, C. F.; Torrecillas, R.; Zurutuza, A., Graphene for tough and electroconductive alumina ceramics. *Journal of the European Ceramic Society* **2013,** *33* (15–16), 3201-3210.

91. Oghbaei, M.; Mirzaee, O., Microwave versus conventional sintering: A review of fundamentals, advantages and applications. *Journal of Alloys and Compounds* **2010,** *494* (1–2), 175-189.

92. Menezes, R. R.; Kiminami, R. H. G. A., Microwave sintering of alumina–zirconia nanocomposites. *Journal of Materials Processing Technology* **2008,** *203* (1–3), 513-517.

93. Clark, D. E.; Sutton, W. H., Microwave Processing of Materials. *Annual Review of Materials Science* **1996,** *26* (1), 299-331.

94. Wang, J.; Zhang, L.; Zhao, G.; Gu, Y.; Zhang, Z.; Zhang, F.; Wang, W., Selective synthesis of boron nitride nanotubes by self-propagation high-temperature synthesis and annealing process. *Journal of Solid State Chemistry* **2011,** *184* (9), 2478-2484.

95. Jankovic, A., Variables affecting the fine grinding of minerals using stirred mills. *Minerals Engineering* **2003,** *16* (4), 337-345.

96. Bluhm, J. I., Slice synthesis of a three dimensional "work of fracture" specimen. *Engineering Fracture Mechanics* **1975,** *7* (3), 593-604.

97. Le Houérou, V.; Sangleboeuf, J. C.; Dériano, S.; Rouxel, T.; Duisit, G., Surface damage of soda–lime–silica glasses: indentation scratch behavior. *Journal of Non-Crystalline Solids* **2003,** *316* (1), 54-63.

98. Yates, B.; Overy, M. J.; Pirgon, O., The anisotropic thermal expansion of boron nitride. *Philosophical Magazine* **1975,** *32* (4), 847-857.

List of Publications

International Conferences

1. **Richa Saggar,** Harshit Porwal, Peter Tatarko, Ivo Dlouhý, Michael J. Reece. Boron Nitride Nanosheets Reinforced Glass Matrix Composites, Material Science Engineering (MSE 2014), September 23 – 25, 2014, Darmstadt, Germany. (Oral)

2. **Richa Saggar,** Harshit Porwal, Peter Tatarko, Ivo Dlouhý, Michael J. Reece. Boron Nitride Nanosheets Reinforced Glass Matrix Composites, Material Science and Technology 2014 (MS&T'14), October 12 – 16, 2014, Pittsburgh, PA, USA. (Oral)

3. **Richa Saggar,** Harshit Porwal, Peter Tatarko, Ivo Dlouhý, Michael J. Reece. Boron Nitride Nanosheets Reinforced Glass Matrix Composites, 17th International Conference on the Strength of Materials (ICSMA 17), August 9 – 14, 2015, Brno, Czech Republic. (Poster)

Journals

1. **Saggar R**., Porwal H., Tatarko P., Dlouhý I., Reece M.J., Boron Nitride Nanosheets Reinforced Amorphous Glass Composite, Advances in applied ceramics 2015, 115 (S1), S26-S33.

2. Tatarko, P.; Grasso, S.; Porwal, H.; Chlup, Z.; **Saggar, R**.; Dlouhy, I.; Reece, M.J., Boron nitride nanotubes as a reinforcement for brittle matrices. Journal of the European Ceramic Society 2014, 34 (14), 3339-3349.

3. Porwal H., Tatarko P., **Saggar R**., Grasso S., Mani M.K. , Dlouhý I. , Dusza J, Reece M.J., Tribological properties of silica–graphene nano-platelet composites, Ceramics International 2014, 40 (8), 12067–12074

4. Porwal H., **Saggar R.,** Tatarko P., Grasso S., Saunders T., Dlouhý I., Reece M.J., Effect of lateral size of Graphene nanosheets on the mechanical properties and machinability of alumina nanocomposites, Ceramics International 2016, 42(6) 7533-7542

Summary

Glasses and ceramics offer several unique characteristics over polymers or metals. However, they suffer from a shortcoming due to their brittle nature, falling short in terms of fracture toughness and mechanical strength. The aim of this work is to reinforce borosilicate glass matrix with reinforcements to increase the fracture toughness and strength of the glass. Boron nitride nanomaterials, i.e. nanotubes and nanosheets have been used as possible reinforcements for the borosilicate glass matrix. The tasks of the thesis are many fold which include:

1. Reinforcement of commercially derived and morphologically different (bamboo like and cylinder like) boron nitride nanotubes in borosilicate glass with the concentration of 0 wt%, 2.5 wt% and 5 wt% by ball milling process. Same process was repeated with reinforcing cleaned boron nitride nanotubes (after acid purification) into the borosilicate glass with similar concentrations.

2. Production of boron nitride nanosheets using liquid exfoliation technique to produce high quality and high aspect ratio nanosheets. These boron nitride nanosheets were reinforced in the borosilicate glass matrix with concentrations of 0 wt%, 2.5 wt% and 5 wt% by ball milling process.

The samples were consolidated using spark plasma sintering. These composites were studied in details in terms of material analysis like thermo-gravimetric analysis, detailed scanning electron microscopy and transmission electron microscopy for the quality of reinforcements etc.; microstructure analysis which include the detailed study of the composite powder samples, the densities of bulk composite samples etc; mechanical properties which include fracture toughness, flexural strength, micro-hardness, Young's modulus etc. and; tribological properties like scratch resistance and wear resistance.

Cleaning process of boron nitride nanotubes lead to reduction in the Fe content (present in boron nitride nanotubes during their production as a catalyst) by ~54%. This leads to an improvement of ~30% of fracture toughness measured by chevron notch technique for 5 wt% boron nitride nanotubes reinforced borosilicate glass. It also contributed to the improvement of scratch resistance by ~26% for the 5 wt% boron nitride nanotubes reinforced borosilicate glass matrix.

On the other hand, boron nitride nanosheets were successfully produced using liquid exfoliation technique with average length was ~0.5 µm and thickness of the nanosheets was between 4-30 layers. It accounted to an improvement of ~45% for both fracture toughness and flexural strength by reinforcing 5 wt% of boron nitride

nanosheets. The wear rates reduced by ~3 times while the coefficient of friction was reduced by ~23% for 5 wt% boron nitride nanosheets reinforcements.

Resulting improvements in fracture toughness and flexural strength in the composite materials were observed due to high interfacial bonding between the boron nitride nanomaterials and borosilicate glass matrix resulting in efficient load transfer. Several toughening and strengthening mechanisms like crack bridging, crack deflection and significant pull-out were observed in the matrix.

It was also observed that the 2D reinforcement served as more promising candidate for reinforcements compared to 1D reinforcements. It was due to several geometrical advantages like high surface area, rougher surface morphology, and better hindrance in two dimensions rather than just one dimension in nanotubes.